HHS Public Access

Author manuscript

Cell Rep. Author manuscript; available in PMC 2024 July 12.

Published in final edited form as:

Cell Rep. 2024 June 25; 43(6): 114258. doi:10.1016/j.celrep.2024.114258.

T-bet deficiency and Hic1 induction override TGF-β-dependency in the formation of CD103+ intestine-resident memory CD8+ T cells

Liwen Wang[1,2], **Shruti Mishra**[1,10], **Kenneth Ka-Ho Fan**[1], **Sara Quon**[4], **Guo Li**[1,5,6,7], **Bingfei Yu**[4,12], **Wei Liao**[1,8,11], **Yong Liu**[5,6,7,9], **Xin Zhang**[5,6,7,9], **Yuanzheng Qiu**[5,6,7,9], **Yue Li**[1], **Ananda W. Goldrath**[4], **Chaoyu Ma**[1,*], **Nu Zhang**[1,3,13,*]

[1]Department of Microbiology, Immunology and Molecular Genetics, Long School of Medicine, University of Texas Health Science Center at San Antonio, San Antonio, TX 78229, USA

[2]Department of Hematology, The Third Xiangya Hospital, Central South University, Changsha, Hunan 410013, China

[3]South Texas Veterans Health Care System, San Antonio, TX 78229, USA

[4]Division of Biological Sciences, University of California, San Diego, La Jolla, CA, USA

[5]Department of Otolaryngology Head and Neck Surgery, Xiangya Hospital, Central South University, 87 Xiangya Road, Changsha, Hunan 410008, China

[6]Otolaryngology Major Disease Research Key Laboratory of Hunan Province, Xiangya Hospital, Central South University, Changsha, Hunan 410008, China

[7]Clinical Research Center for Laryngopharyngeal and Voice Disorders in Hunan Province, Xiangya Hospital, Central South University, Changsha, Hunan 410008, China

[8]Department of Dermatology, Hunan Key Laboratory of Medical Epigenomics, The Second Xiangya Hospital, Central South University, Changsha, Hunan 410011, China

[9]National Clinical Research Center for Geriatric Disorders, Xiangya Hospital, Central South University, Changsha, Hunan 410008, China

[10]Present address: Department of Cancer Immunology and Virology, Dana-Farber Cancer Institute, Harvard Medical School, Boston, MA 02215, USA

[11]Present address: Department of Dermatology, Hunan Children's Hospital, 86 Ziyuan Road, Changsha, Hunan 410007, China

[12]Present address: Department of Microbiology and Immunology, Keck School of Medicine of University of Southern California, 2011 Zonal Ave. Los Angeles, CA 90033, USA

*Correspondence: mac4@uthscsa.edu (C.M.), zhangn3@uthscsa.edu (N.Z.).

AUTHOR CONTRIBUTIONS

Conceptualization, C.M., A.W.G., X.Z., Q.Z., and N.Z.; investigation, L.W., S.M., K.K.-H.F., S.Q., G.L., B.Y., W.L., Y. Liu, Y. Li, and C.M.; bioinformatics, L.W., S.Q., and K.K.-H.F.; writing – original draft, L.W., C.M., and N.Z.; writing – reviewing & editing, L.W., C.M., A.W.G., and N.Z.; supervision, A.W.G., C.M., and N.Z.; funding acquisition, A.W.G. and N.Z.

SUPPLEMENTAL INFORMATION

Supplemental information can be found online at https://doi.org/10.1016/j.celrep.2024.114258.

[13]Lead contact

SUMMARY

Transforming growth factor β (TGF-β) represents a well-established signal required for tissue-resident memory T cell (T_{RM}) formation at intestinal surfaces, regulating the expression of a large collection of genes coordinately promoting intestinal T_{RM} differentiation. The functional contribution from each TGF-β-controlled transcription factor is not entirely known. Here, we find that TGF-β-induced T-bet downregulation and Hic1 induction represent two critical events during intestinal T_{RM} differentiation. Importantly, T-bet deficiency significantly rescues intestinal T_{RM} formation in the absence of the TGF-β receptor. Hic1 induction further strengthens T_{RM} maturation in the absence of TGF-β and T-bet. Our results reveal that provision of certain TGF-β-induced molecular events can partially replace TGF-β signaling to promote the establishment of intestinal T_{RM}s, which allows the functional dissection of TGF-β-induced transcriptional targets and molecular mechanisms for T_{RM} differentiation.

In brief

Wang et al. find that T-bet deficiency significantly rescues intestine T_{RM} differentiation in TGF-βR-KO cells. Suppressing the type 17 program or enforced expression of Hic1 further boosts T_{RM} formation in T-bet/TGF-βR DKO T cells. These results show the key molecular events downstream of TGF-β signaling during intestine T_{RM} differentiation.

Graphical abstract

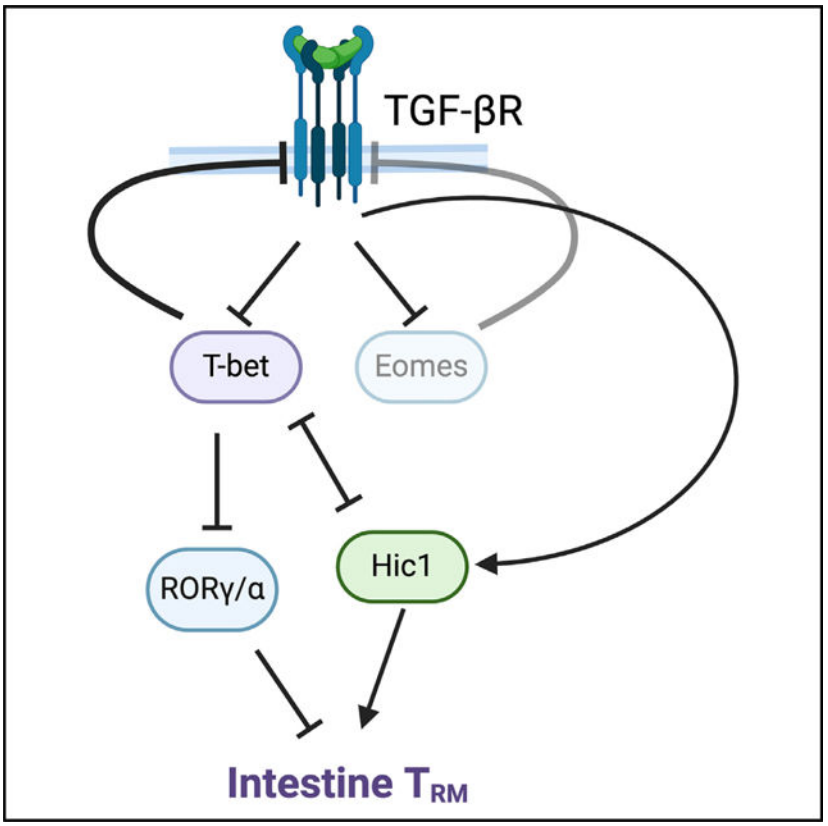

INTRODUCTION

Tissue-resident memory T cells (T_{RM}s) are one of the key adaptive immune components and the first line of defense in mucosal tissues.[1–3] To form mucosal T_{RM}s, a subset of effector T cells migrate to the mucosal surface, receive local signals, and initiate a unique differentiation program. Mucosal T_{RM}s often express the surface markers CD69 and CD103. It is generally accepted that transforming growth factor β (TGF-β) is required for the establishment of the mucosal T_{RM} population, especially for $CD103^+$ T_{RM}s, since CD103 (encoded by *Itgae*) is a direct target of TGF-β signaling in $CD8^+$ T cells.[4–9] However, the function of individual molecular targets downstream of TGF-β signaling is less clear during T_{RM} establishment.

T-box transcription factors T-bet (encoded by *Tbx21*) and Eomes (encoded by *Eomes*) play essential roles in effector and memory $CD8^+$ T cell differentiation.[10,11] It has been demonstrated that TGF-β signaling downregulates the expression of T-bet and Eomes during skin T_{RM} differentiation[12] and forced expression of either T-bet or Eomes significantly suppresses skin T_{RM} formation. Downregulation of T-box transcription factors leads to enhanced TGF-β receptor expression, which results in a feedforward loop to reinforce TGF-β-dependent T_{RM} differentiation.[12] Considering the fact that Eomes cannot replace T-bet in effector $CD8^+$ T cells,[13] it remains unknown whether T-bet and Eomes play equivalent roles in T_{RM} differentiation. Importantly, mature T_{RM}s almost completely turn off the expression of Eomes while carrying a low level of T-bet expression to maintain responsiveness to

interleukin (IL)-15.[12] However, IL-15 dependency is a tissue-specific feature for T_{RM}s. In contrast to IL-15-dependent skin T_{RM}s, intestinal T_{RM}s are IL-15 independent.[14] Whether TGF-β-dependent quenching of T-box transcription factors is the central hub of the TGF-β-controlled T_{RM} differentiation program and whether the same mechanisms are operating at the intestinal surface remain elusive. Recently, it was shown that the transcriptional repressor Hic1 acts as a specific regulator of intestinal T_{RM} differentiation.[15] However, the functional interaction between Hic1 and other T_{RM}-promoting factors is not entirely clear.

Here, using genetic models, we show that T-bet deficiency, but not Eomes deficiency, significantly rescues the differentiation of $CD103^+$ intestinal T_{RM}s in the absence of TGF-β receptor. T-bet deficiency allows the induction of the tissue-residency program at both transcriptional and epigenetic levels in TGF-β-receptor-deficient cells. T-bet deficiency induces a type 17 program in T_{RM}s. Suppressing the type 17 program further boosts T_{RM} differentiation. Interestingly, T-bet deficiency cannot fully restore Hic1-controlled intestinal T_{RM} differentiation. Forced expression of *Hic1* further enhances the formation of $CD103^+$ T_{RM} in the absence of both T-bet and TGF-β receptor. In contrast, forced induction of *Hic1* in TGF-β-receptor-deficient cells only improves the differentiation of $CD69^+CD103^-$, but not $CD103^+$, T_{RM}s at the intestinal surface. Together, our genetic models have revealed the function of essential events in the TGF-β-induced intestine T_{RM} differentiation program.

RESULTS

TGF-β signaling downregulates the expression of T-bet and Eomes during gut T_{RM} differentiation

To dissect the components of the TGF-β-induced T_{RM} differentiation program, we first focused on T-box transcription factors T-bet and Eomes. We employed lymphocytic choriomeningitis virus (LCMV) acute infection model and TGF-β receptor II conditional-knockout (KO) (*Tgfbr2*$^{f/f}$ distal *Lck*-Cre,[16] hereafter referred to as *Tgfbr2*$^{-/-}$) P14 TCR transgenic mice, which carried $CD8^+$ T cells specific for LCMV epitope H-$2D^b$-$GP_{33–41}$. As illustrated in Figure S1A, naive P14 T cells carrying distinct congenic markers were isolated from wild-type (WT) control (CD45.1/1) and *Tgfbr2*$^{-/-}$ mice (CD45.1/2), mixed at a 1:1 ratio and adoptively co-transferred into unmanipulated sex-matched C57BL/6 (B6, CD45.2/2) recipient mice followed by LCMV Armstrong infection. In this system, WT and *Tgfbr2*$^{-/-}$ P14 T cells were compared side by side in the same WT environment. Consistent with published results for T_{RM} isolated from the skin, we observed TGF-β-dependent downregulation of both T-bet and Eomes during gut T_{RM} differentiation (Figures S1B–S1E). Importantly, the downregulation of both T-bet and Eomes occurred before the induction of CD103 expression (Figures S1B and S1C). Further, during *in vitro* T cell activation, TGF-β inhibited the expression of both T-bet and Eomes in purified WT $CD8^+$ T cells (Figure S1F). Thus, TGF-β-controlled downregulation of T-box transcription factors represents an early event for intestinal T_{RM} differentiation.

T-bet and Eomes deficiency alters circulating effector and memory $CD8^+$ T cells

To directly address the question of whether failed downregulation of T-bet and/or Eomes in *Tgfbr2*$^{-/-}$ cells is responsible for defective T_{RM} formation, we generated double-

conditional-KO mouse strains for TGF-βR II and T-bet (i.e., *Tgfbr2*$^{f/f}$ *Tbx21*$^{f/f}$ d*Lck*-Cre, hereafter referred to as *Tgfbr2*$^{-/-}$ *Tbx21*$^{-/-}$) as well as TGF-βR II and Eomes (i.e., *Tgfbr2*$^{f/f}$ *Eomes*$^{f/f}$ d*Lck*-Cre, simplified as *Tgfbr2*$^{-/-}$ *Eomes*$^{-/-}$). Furthermore, we bred all double-and single-KO strains with P14 TCR transgenic mice carrying congenic markers so that we could perform the same co-transfer experiments as in Figure S1A to carry out a side-by-side comparison of virus-specific CD8$^+$ T cells with different genetic manipulation in a WT environment.

As illustrated in Figures S2A and S3A, naive P14 T cells isolated from WT plus one of the single- and double-KO mice were mixed at a 1:1 ratio and co-transferred into B6 recipients followed by LCMV arm infection. First, we examined circulating CD8$^+$ T cells isolated from the spleen. Consistent with previous publications, *Tgfbr2*$^{-/-}$ CD8$^+$ T cells exhibited a slight reduction of initial expansion and increased KLRG1$^+$ subset.[6] Interestingly, Eomes deficiency largely corrected these defects as *Tgfbr2*$^{-/-}$ *Eomes*$^{-/-}$ P14 T cells exhibited expansion and KLRG1 expression comparable to co-transferred WT controls (Figures S2B, S2C, and S2E). In contrast, T-bet deficiency severely impaired the initial expansion of effector P14 T cells as seen in both T-bet single-KO (Figure S3B) and *Tgfbr2*$^{-/-}$ *Tbx21*$^{-/-}$ cells (Figure S2B). As expected, T-bet deficiency almost completely abolished KLRG1$^+$ subset (Figures S2D, S2E, and S3C).[10,17,18] Using a different set of markers (CD62L and CD127) to define circulating memory T cells, T-bet-single and *Tgfbr2*$^{-/-}$ *Tbx21*$^{-/-}$ cells exhibited similarly enhanced T_{EM} population and greatly reduced terminal T_{EM} (T-T_{EM}) subset (Figure S2F).[19] Further, expression of the well-established T-bet target gene, CXCR3, was severely defective for *Tgfbr2*$^{-/-}$ *Tbx21*$^{-/-}$ cells (Figure S2D), validating our genetic models. Together with certain expected defects, the double-KO P14 T cells differentiated into circulating effector and memory T cells.

T-bet deficiency, but not Eomes deficiency, corrects gut T_{RM} differentiation in the absence of TGF-βR

Next, we focused on P14 T cells isolated from the small intestine. When T-bet-single or Eomes-single conditional-KO cells were examined, enhanced induction of T_{RM} markers CD69 and CD103 was observed at early time points (e.g., day 5 and day 7) (Figures S3D and S3E). However, at memory phase (≥d30), the phenotypic difference between WT and *Tbx21*$^{-/-}$ or WT and *Eomes*$^{-/-}$ cells was either subtle or not significant (Figures S3D and S3E). Thus, we concluded that T-bet or Eomes deficiency accelerated gut T_{RM} differentiation, consistent with the observation in skin T_{RM} differentiation.[12] Interestingly, we often detected more dramatic changes in T-bet KO compared with Eomes KO (Figures S3B, S3D, and S3E).

Next, we examined whether T-bet or Eomes deficiency could overcome the blockade of intestinal T_{RM} differentiation in the absence of TGF-βR. When comparing *Tgfbr2*$^{-/-}$ vs. *Tgfbr2*$^{-/-}$ *Eomes*$^{-/-}$ gut T_{RM} differentiation, we did not detect any significant difference in either the total population size or the induction of CD69 and CD103 in small intestine intraepithelial lymphocyte (SI-IEL) compartment (Figures 1A, 1B, 1D, and 1E). In contrast, when examining *Tgfbr2*$^{-/-}$ *Tbx21*$^{-/-}$ vs. *Tgfbr2*$^{-/-}$ cells, there was a clear and significant rescue of the population size as well as phenotypic markers of gut T_{RM} (Figures 1A, 1C,

1D, and 1E). We could detect a significant rescue of gut T_{RM} differentiation as early as day 7 post infection and a gradual increase in the proportion of $CD69^+CD103^+$ subset in *Tgfbr2*$^{-/-}$ *Tbx21*$^{-/-}$ cells (Figures 1C–1E). Together, we conclude that T-bet deficiency, but not Eomes deficiency, partially rescues SI-IEL T_{RM} differentiation in the absence of TGF-β receptor.

Next, we performed a side-by-side comparison of WT, *Tgfbr2*$^{-/-}$, *Tgfbr2*$^{-/-}$ *Tbx21*$^{-/-}$, and *Tbx21*$^{-/-}$ P14 T cell in the same experiments and expanded the analysis to include lamina propria (LP) and Peyer's patches (PPs). As expected, *Tgfbr2*$^{-/-}$ cells exhibited severe defects in T_{RM} differentiation in all intestinal tissues (Figures 2D and 2G). *Tbx21*$^{-/-}$ T_{RM}s showed similar or slightly increased frequency and number of $CD69^+CD103^+$ cells compared with WT controls at memory time points (Figures 2B–2H). *Tgfbr2*$^{-/-}$ *Tbx21*$^{-/-}$ exhibited a partial, but significant, rescue of both population size and surface markers of gut T_{RM}s, including CD69 and CD103, but not CD49a and CXCR3 (Figures 2B–2H). Together, T-bet deficiency, but not Eomes deficiency, significantly rescues intestinal T_{RM} differentiation in the absence of TGF-β receptor.

T-bet deficiency allows TGF-β-independent differentiation of gut T_{RM}s

With this surprising rescue phenotype, we would like to validate the deletion efficiency first to rule out the possibility that some cells escaped Cre-mediated deletion in the intestinal T_{RM} compartment. First, we examined *Tbx21* locus. When gated on IEL P14 T cells, the expression of T-bet was dramatically reduced in both *Tbx21*$^{-/-}$ and *Tgfbr2*$^{-/-}$ *Tbx21*$^{-/-}$ cells at protein level (Figure 2A). Further, when sorted *Tgfbr2*$^{-/-}$ *Tbx21*$^{-/-}$ IEL P14 T cells were subjected to RNA sequencing (RNA-seq) analysis, the expression of *Tbx21* was almost completely abolished (Figure S4E and housekeeping control in Figure S4G). Next, we focused on *Tgfbr2* locus. To this end, we first compared the expression of CD103 on naive $CD8^+$ T cells in uninfected animals. WT and *Tbx21*$^{-/-}$ $CD8^+$ T cells expressed comparable levels of CD103. In contrast, both *Tgfbr2*$^{-/-}$ and *Tgfbr2*$^{-/-}$ *Tbx21*$^{-/-}$ $CD8^+$ T cells were almost completely devoid of CD103 expression (Figure S4A). Further, we employed an *in vitro* culture system. Briefly, naive P14 T cells were isolated from WT, *Tbx21*$^{-/-}$, *Tgfbr2*$^{-/-}$, and *Tgfbr2*$^{-/-}$ *Tbx21*$^{-/-}$ mice, activated by TCR/CD28 stimulation and cultured in IL-2 with added TGF-β or TGF-β neutralizing antibody. Four days later, only WT and *Tbx21*$^{-/-}$ P14 T cells expressed CD103 in a TGF-β-dependent manner, while *Tgfbr2*$^{-/-}$ and *Tgfbr2*$^{-/-}$ *Tbx21*$^{-/-}$ cells did not induce CD103 expression (Figure S4B). To further validate the findings, we used the well-established *in vivo* priming + *ex vivo* culture system (Figure S4C).[20,21] As shown in Figure S4D, *in vivo*-primed WT P14 T cells responded to TGF-β and induced CD103 expression. *Tbx21*$^{-/-}$ cells exhibited greatly enhanced response to TGF-β, which is consistent with previous findings.[22] In contrast, *Tgfbr2*$^{-/-}$ and *Tgfbr2*$^{-/-}$ *Tbx21*$^{-/-}$ cells failed to upregulate CD103 in this setting. Lastly, when sorted *Tgfbr2*$^{-/-}$ *Tbx21*$^{-/-}$ IEL P14 T cells were examined by RNA-seq analysis, a specific loss of transcripts starting from exon 5 was detected (Figure S4F), which was the floxed exon in our conditional-KO model. Based on this set of experiments, we concluded that there was no escaped deletion in either *Tbx21* or *Tgfbr2* loci. T-bet deficiency allows TGF-β-independent differentiation of gut T_{RM}s after arrival at local intestinal tissues.

T-bet deficiency cannot rescue *Tgfbr2*$^{-/-}$ T_{RM} formation in the kidney and salivary glands

To determine whether the rescue phenotype is intestine specific or a general phenomenon, we examined kidney and salivary glands (SGs). As we and others have published,[23,24] $CD8^+$ T_{RM} differentiation and maturation in both kidney and SG are TGF-β-dependent. Kidney T_{RM}s represent non-barrier tissue T_{RM}s and often lack the expression of CD103. In contrast, SG T_{RM}s reside in an IEL compartment and carry CD103 expression. Using the same LCMV infection system, we found that the population and phenotype of *Tgfbr2*$^{-/-}$ *Tbx21*$^{-/-}$ T_{RM}s were indistinguishable from *Tgfbr2*$^{-/-}$ ones in both kidney and SG (Figures S2G and S2H). Thus, T-bet deficiency rescues *Tgfbr2*$^{-/-}$ T_{RM} formation in an intestine-specific manner.

Altered effector program in *Tgfbr2*$^{-/-}$*Tbx21*$^{-/-}$ T_{RM}s

Because T-box transcription factors have well-established roles in the CD8 effector program, we addressed whether *Tgfbr2*$^{-/-}$ *Tbx21*$^{-/-}$ gut T_{RM}s were functional. For this purpose, WT plus *Tgfbr2*$^{-/-}$ *Tbx21*$^{-/-}$ P14 T cells or WT plus single-KO controls were co-transferred into WT recipients followed by LCMV infection (Figure 3A). *Eomes*$^{-/-}$ memory T cells exhibited similar effector functions to co-transferred WT controls in both spleen and SI-IELs (Figures 3B–3D). Compared to WT controls, both *Tbx21*$^{-/-}$ and *Tgfbr2*$^{-/-}$ *Tbx21*$^{-/-}$ memory T cells produced reduced levels of interferon (IFN)-γ and granzyme A in the spleen (Figures 3B, 3F, 3H, and S5A). However, in the SI-IEL compartment, T-bet deficiency had minimal impact on IFN-γ and granzyme A production (Figures 3B, 3G, 3H, and S5B). Both *Tbx21*$^{-/-}$ and *Tgfbr2*$^{-/-}$ *Tbx21*$^{-/-}$ memory T cells produced similar levels of tumor necrosis factor (TNF) and significantly increased amounts of IL-2 and IL-17 in both spleen and SI-IEL compartments (Figures 3C–3H). Together, *Tbx21*$^{-/-}$ and *Tgfbr2*$^{-/-}$ *Tbx21*$^{-/-}$ memory $CD8^+$ T cells exhibit enhanced type 17 response in both circulating memory T cells and T_{RM}s. In contrast, T-bet was only required for the optimal type 1 effector program in circulating memory T cells but not in small intestine T_{RM}s.

Type 17 program inhibits gut T_{RM} differentiation in the absence of T-bet

It has been reported that T-bet deficiency promotes a RORγ-dependent type 17 response in $CD8^+$ T_{RM}s.[12,18] Indeed, we could detect a significant portion of P14 T cells producing IL-17 in the absence of T-bet (Figure 3). This finding was not T_{RM} specific as IL-17^+ cells were present in both spleen and IEL. To determine whether this type 17 program was involved in T_{RM} differentiation in the absence of T-bet, we first examined the expression of RORγ in gut T_{RM}s. Compared with WT controls, both *Tbx21*$^{-/-}$ and *Tgfbr2*$^{-/-}$ *Tbx21*$^{-/-}$ T_{RM}s carried significantly increased expression of RORγ (Figures 4A and 4B). Interestingly, in *Tgfbr2*$^{-/-}$ *Tbx21*$^{-/-}$ cells, the expression of RORγ was greatly enhanced in $CD103^-$ subset compared with $CD103^+$ counterpart (Figures 4A and 4B), suggesting that RORγ may not be required for or may suppress $CD103^+$ T_{RM}s in this setting. To directly address whether RORγ was involved in *Tbx21*$^{-/-}$ gut T_{RM} differentiation, we generated T-bet and RORγ double-KO mice carrying P14 TCR transgene (i.e., *Rorc*$^{-/-}$ *Tbx21*$^{-/-}$). As illustrated in Figure 4C, WT plus *Tbx21*$^{-/-}$ or WT plus *Rorc*$^{-/-}$ *Tbx21*$^{-/-}$ P14 T cells were adoptively co-transferred into WT recipients followed by LCMV infection. As expected, *Rorc*$^{-/-}$ *Tbx21*$^{-/-}$ cells completely lost RORγ expression (Figure 4D). However, we could

not detect major defects in gut T_{RM} differentiation for *Rorc*$^{-/-}$ *Tbx21*$^{-/-}$ cells (Figure 4E). Indeed, there was a slight but significant increase of CD103 expression in *Rorc*$^{-/-}$ *Tbx21*$^{-/-}$ cells (Figure 4E).

Next, to directly test whether the type 17 program is required for *Tgfbr2*$^{-/-}$ *Tbx21*$^{-/-}$ T_{RM} formation, we employed a CRISPR-Cas9-based system.[25] As shown in Figure 4F, naive P14 T cells were isolated from two congenically distinct *Tgfbr2*$^{-/-}$ *Tbx21*$^{-/-}$ mice. A pre-made control single guide RNA (sgRNA)/Cas9 complex was delivered into CD45.1/1 P14, while *Rorc*- or *Rora*-targeting sgRNA/Cas9 was delivered into CD45.1/2 cells. After electroporation-mediated sgRNA/Cas9 delivery, control- and targeting-sgRNA/Cas9-treated naive P14 T cells were 1:1 mixed, adoptively transferred into B6 recipients, followed by LCMV infection. To be noted, in this system, no *in vitro* T cell activation is required for sgRNA/Cas9 delivery. P14 T cells are primed *in vivo* following LCMV infection. Further, we could achieve high targeting efficiency in intestinal T_{RM}s (Figure 4H). Four weeks post infection, we observed significant enrichment of *Rorc*$^{-/-}$ *Tgfbr2*$^{-/-}$ *Tbx21*$^{-/-}$ and *Rora*$^{-/-}$ *Tgfbr2*$^{-/-}$ *Tbx21*$^{-/-}$ P14s over the co-transferred control sgRNA-treated *Tgfbr2*$^{-/-}$ *Tbx21*$^{-/-}$ ones in the SI-IEL compartment (Figure 4G). Both *Rorc* and *Rora* deletion enhanced CD103 expression in *Tgfbr2*$^{-/-}$ *Tbx21*$^{-/-}$ T_{RM}s in the small intestine (Figure 4I). In summary, although T-bet deficiency leads to enhanced type 17 program, *Rorc/Rora*-controlled type 17 program suppresses CD103^{+} T_{RM} formation in the small intestine.

T-bet deficiency partially rescues gut *Tgfbr2*$^{-/-}$ T_{RM} differentiation at the transcriptional level

To further characterize *Tgfbr2*$^{-/-}$ *Tbx21*$^{-/-}$ T_{RM}, we determined their transcriptional profiles. Briefly, using fluorescence-activated cell sorting (FACS), we sorted different subsets of P14 T cells isolated from SI-IEL compartment together with a WT splenic P14 T cell subset (i.e., KLRG1^{-}) as a circulating memory T cell control. All sorted cells were subjected to bulk RNA-seq analysis. Using principal-component analysis, circulating memory T cells were separated from all SI-IEL subsets based on PC1, accounting for 57% of variance (Figure 5A). Along PC1, WT CD103^{+} and *Tbx21*$^{-/-}$ CD103^{+} IEL cells were similarly positioned, while *Tgfbr2*$^{-/-}$ *Tbx21*$^{-/-}$ CD103^{+} ones were situated between T_{RM}s and circulating controls (Figure 5A). We did observe difference along PC2 (19% variance) between different CD103^{+} IEL subsets (Figure 5A). When focused on established circulating and resident gene signatures, *Tgfbr2*$^{-/-}$ *Tbx21*$^{-/-}$ IELs carried a gene set variation analysis (GSVA) score between T_{RM}s (including both WT and *Tbx21*$^{-/-}$ IELs) and circulating T cells (Figure 5B). This finding was further validated by unsupervised clustering in heatmaps focusing on T_{Cir} and T_{RM} signature genes (Figure S6). When performing gene set enrichment analysis (GSEA) to compare different IEL subsets vs. WT splenic T cells for T_{Cir} and T_{RM} signatures, all CD103^{+} subsets (including WT, *Tbx21*$^{-/-}$, and *Tgfbr2*$^{-/-}$ *Tbx21*$^{-/-}$) were positively enriched for T_{RM} signature and negatively enriched for the T_{Cir} one (Figure 5C top row). When comparing CD69^{+}CD103^{-} IEL subsets and splenic T cells, we observed similar T_{RM}-like enrichment for WT and *Tgfbr2*$^{-/-}$ *Tbx21*$^{-/-}$ cells (Figure 5C bottom row). Interestingly, *Tgfbr2*$^{-/-}$ CD69^{+}CD103^{-} IEL subsets were also positively enriched for T_{RM} signature and trending negatively enriched for the T_{Cir} one (Figure 5C, bottom right). When the *Tgfbr2*$^{-/-}$ CD69^{+}CD103^{-} subset was compared with its WT counterpart, we

detected significant enrichment of T_{Cir} in *Tgfbr2*$^{-/-}$ cells, while the T_{RM} signature was comparable (Figure 5D left). When *Tgfbr2*$^{-/-}$ CD69^{+}CD103^{-} cells were compared with WT CD103^{+} T_{RM}, WT T_{RM}s were positively enriched for T_{RM} and negatively enriched for T_{Cir} signature (Figure 5D right). These results demonstrate that *Tgfbr2*$^{-/-}$ cells can initiate but cannot complete the T_{RM} differentiation program. Importantly, both *Tgfbr2*$^{-/-}$ *Tbx21*$^{-/-}$ CD69^{+}CD103^{+} and CD69^{+}CD103^{-} cells exhibited a T_{RM} GSEA pattern (Figure 5C).

When comparing differentially expressed genes (DEGs) between various T_{RM} subsets and circulating controls, we identified seven clusters of genes (Figure S7A). The common cluster shared by WT, *Tbx21*$^{-/-}$, and *Tgfbr2*$^{-/-}$ *Tbx21*$^{-/-}$ T_{RM}s was highly enriched for the biological processes related to the digestion system and actin-based cell projections (Figures S7B, C5). This finding supports the tissue specificity of this rescue phenotype demonstrated in Figures S2G and S2H. Together, consistent with phenotypic characterization, T-bet deficiency partially rescues the differentiation of intestinal T_{RM}s in the absence of TGF-β receptor at the transcriptional level.

T-bet-controlled Tcf-1 expression is not involved in intestinal T_{RM} formation in *Tgfbr2*$^{-/-}$*Tbx21*$^{-/-}$ cells

In addition to the type 17 program, we were interested in other transcriptional programs induced by T-bet deficiency. Interestingly, we detected significantly increased expression of *Tcf7*. Using flow cytometry, we validated that, for both spleen memory T cells and IEL T_{RM}s, the expression of Tcf-1 (encoded by *Tcf7*) was significantly enhanced in the absence of T-bet (Figure S8A). To directly test whether the induction of Tcf-1 was responsible for T-bet deficiency-mediated T_{RM} rescue, we employed a similar CRISPR-Cas9 system to Figure 4F. Briefly, naive P14 T cells were isolated from two congenically distinct *Tgfbr2*$^{-/-}$ *Tbx21*$^{-/-}$ mice. One population of P14 T cells received control sgRNA/Cas9 and the other received *Tcf7*-targeting sgRNA/Cas9. Treated P14 T cells were mixed at a 1:1 ratio and adoptively co-transferred into B6 recipients followed by LCMV infection (Figure S8B). As shown in Figure S8C, sgRNA/Cas9-mediated deletion almost completely abolished Tcf-1 induction in the IEL compartment. However, no major differences were detected in gut T_{RM} differentiation except for a slight increase of CD103 expression at an early time point (Figures S8D and S8E). Together, the induction of Tcf-1 is not apparently required for T_{RM} formation in *Tgfbr2*$^{-/-}$ *Tbx21*$^{-/-}$ cells.

T-bet deficiency partially rescues gut *Tgfbr2*$^{-/-}$ T_{RM} differentiation at the epigenetic level

Next, we examined whether T-bet deficiency had any impacts at the epigenetic level. To this end, P14 subsets were FACS sorted from SI-IEL compartment and subjected to assay for transposase-accessible chromatin with sequencing (ATAC-seq) analysis. When focusing on the transcription start site (TSS) region of all T_{RM} signature genes, we could detect significant defects in *Tgfbr2*$^{-/-}$ cells, which were largely corrected in *Tgfbr2*$^{-/-}$ *Tbx21*$^{-/-}$ cells (Figure S9A dark red arrow). Further, motif enrichment analysis was largely consistent with our previous analysis, i.e., reduced T-bet, enhanced Tcf-1/Lef1 motif, and increased ROR-γ motif enrichment in the cells lacking T-bet, and decreased Smad4 motif enrichment in the cells lacking TGF-β receptor (Figure S9B). Narrowing down to individual genes, we identified several categories of gene loci. First, in multiple genomic regions

harboring residency-related genes, *Tgfbr2*$^{-/-}$ *Tbx21*$^{-/-}$ CD69^{+}CD103^{+} cells exhibited an intermediate phenotype between *Tgfbr2*$^{-/-}$ CD69^{-} non-T_{RM}s and T_{RM}s (including both WT and *Tbx21*$^{-/-}$ CD69^{+}CD103^{+}). This category included *Itgae*, *Rgs1*, *Runx3*, *Litaf*, *Cdh1*, and *Xcl1* (Figures 5E and S9F). Second, for some genomic regions, *Tgfbr2*$^{-/-}$ *Tbx21*$^{-/-}$ CD69^{+}CD103^{+} cells exhibited a similar phenotype to T_{RM}s (including both WT and *Tbx21*$^{-/-}$ CD69^{+}CD103^{+}) and distinct from *Tgfbr2*$^{-/-}$ CD69^{-} non-T_{RM}s. This category included *S1pr5* (5′ region of the promoter), *Eomes*, *Klrg1* (promoter region), *S1pr1*, *Sell*, and *Cd69* (Figures 5E, S9C, S9E, and S9F). Finally, there were some regions exhibiting a T-bet-dependent pattern; i.e., *Tgfbr2*$^{-/-}$ CD69^{-} were similar to WT CD69^{+}CD103^{+} cells, while *Tbx21*$^{-/-}$ CD69^{+}CD103^{+} were similar to *Tgfbr2*$^{-/-}$ *Tbx21*$^{-/-}$ ones. The last category included the promoter region of *S1pr5*, *Tbx21*, *Zeb2*, distal region of *Klrg1*, and type 17-related genes *Il17f* and *Ccr6* (Figures 5E, S9C, S9D, and S9E). Together, our ATAC-seq results largely support the conclusion that T-bet deficiency partially rescues *Tgfbr2*$^{-/-}$ intestinal T_{RM} differentiation at an epigenetic level.

Hic1 further boosts CD103^{+} T_{RM} formation in the absence of T-bet

Since T-bet deficiency only partially overcame TGF-β dependency in gut T_{RM} differentiation, we wanted to identify key transcription regulator(s) missing in *Tgfbr2*$^{-/-}$ *Tbx21*$^{-/-}$ cells. Transcription repressor Hic1 has recently been demonstrated to be a key regulator for T_{RM} differentiation in an intestine-specific manner.[15] We were curious whether *Hic1* induction represented another downstream event of TGF-β signaling and a missing factor for *Tgfbr2*$^{-/-}$ *Tbx21*$^{-/-}$ T_{RM} formation.

First, we confirmed that *Hic1* was induced by TGF-β during CD8^{+} T cell activation *in vitro* (Figure 6A). Next, we measured the expression of *Hic1* at the protein level. Circulating T cells expressed minimal levels of Hic1, while IEL T_{RM}s exhibited a dramatic induction of Hic1 in a TGF-β-dependent manner (Figure 6B). T-bet deficiency partially rescued the defective expression of Hic1 in *Tgfbr2*$^{-/-}$ cells. Interestingly, compared with WT controls, *Tbx21*$^{-/-}$ T_{RM}s expressed slightly but significantly increased levels of Hic1 (Figure 6B). Together, optimal Hic1 expression requires both TGF-β signal and T-bet downregulation.

Subsequently, we would like to test whether reduced Hic1 expression in *Tgfbr2*$^{-/-}$ *Tbx21*$^{-/-}$ cells was responsible for their suboptimal differentiation compared with WT controls. To this end, WT P14 T cells were transduced with an empty retroviral vector (RV) and *Tgfbr2*$^{-/-}$ *Tbx21*$^{-/-}$ P14 T cells were transduced with a retroviral vector carrying *Hic1* cDNA (*Hic1* overexpression [OE]). After spin transduction, WT and *Tgfbr2*$^{-/-}$ *Tbx21*$^{-/-}$ P14 T cells were mixed 1:1 and adoptively transferred into B6 recipients immediately followed by LCMV infection. In this system, we were able to compare four subsets of P14 T cells isolated from the same tissue (i.e., WT, WT + empty RV, *Tgfbr2*$^{-/-}$ *Tbx21*$^{-/-}$, and *Tgfbr2*$^{-/-}$ *Tbx21*$^{-/-}$ + *Hic1* OE). Indeed, *Hic1* OE significantly boosted both CD69 and CD103 expression in intestinal *Tgfbr2*$^{-/-}$ *Tbx21*$^{-/-}$ cells (Figures 6C, 6E, and 6F). We have demonstrated that IL-18 receptor downregulation is associated with the establishment of tissue residency.[23] In addition to CD69 and CD103, *Hic1* OE facilitated IL-18R downregulation in *Tgfbr2*$^{-/-}$ *Tbx21*$^{-/-}$ cells (Figure 6D). When using splenic P14 subsets as an internal reference to calculate the relative abundance of IEL P14 population, we found that *Hic1* OE significantly

enhanced the total population of *Tgfbr2*$^{-/-}$ *Tbx21*$^{-/-}$ IEL T_{RM}s (Figure 6G left). When directly examining the total population size of each subset, *Hic1* OE cells were highly enriched in the SI-IEL compartment compared with the spleen (Figure 6H left). Together, forced expression of *Hic1* markedly enhances the differentiation of intestinal *Tgfbr2*$^{-/-}$ *Tbx21*$^{-/-}$ T_{RM}s.

Considering the impressive impacts of *Hic1* OE in *Tgfbr2*$^{-/-}$ *Tbx21*$^{-/-}$ T_{RM}s, we wondered whether *Hic1* could directly boost intestinal T_{RM} formation in *Tgfbr2*$^{-/-}$ cells. Interestingly, using a similar retrovirus system, *Hic1* OE was able to boost CD69 expression as well as the total population size of *Tgfbr2*$^{-/-}$ cells (Figure 6G right, 6H right, 6I, and 6J). Remarkably, the expression of CD69 in *Hic1* OE *Tgfbr2*$^{-/-}$ IEL cells was comparable to that of WT controls (Figures 6I and 6J). In stark contrast, *Hic1* OE led to no detectable improvement of CD103 expression in *Tgfbr2*$^{-/-}$ cells (Figures 6I and 6K). At day 28 post infection, *Hic1* OE even reduced CD103 expression (Figure 6K), likely due to the strong selection for retention in IEL compartment favors undeleted and therefore CD103^{+} "*Tgfbr2*$^{-/-}$" cells while *Hic1* OE boosts CD69 levels and thus alleviates this selection pressure.

To rule out the possibility that *Hic1* OE only affected a few T_{RM}-associated surface markers, we performed bulk RNA-seq analysis on FACS-sorted SI-IEL P14 T cells. Unsupervised principal-component analysis (PCA) plot showed that along PC1 (42% variance), *Hic1* OE *Tgfbr2*$^{-/-}$ *Tbx21*$^{-/-}$ IEL cells almost overlapped with WT IEL controls (Figure 7A). Along PC2 (23% variance), we did observe a separation between WT, *Tgfbr2*$^{-/-}$ *Tbx21*$^{-/-}$, and *Tgfbr2*$^{-/-}$ *Tbx21*$^{-/-}$ *Hic1* OE subsets (Figure 7A). When narrowed down to the established T_{RM} and T_{Cir} signatures, an interesting pattern emerged. *Hic1* OE did not significantly enhance T_{RM} signature in *Tgfbr2*$^{-/-}$ *Tbx21*$^{-/-}$ cells (Figure 7B blue line and 7E). Instead, *Hic1* OE significantly reduced T_{Cir} signature in *Tgfbr2*$^{-/-}$ *Tbx21*$^{-/-}$ cells (Figure 7B red and 7D). *Tgfbr2*$^{-/-}$ *Tbx21*$^{-/-}$ *Hic1* OE IEL cells carried decreased T_{Cir} signature even when compared with WT IEL (Figure 7C red). Bio-logical process Gene Ontology analysis revealed that *Hic1* OE controlled multiple pathways, including leukocyte adhesion, immune response, and regulation of DNA-binding transcription factor activity (Figure S7C). Together, *Hic1* OE boosts intestinal T_{RM} formation in *Tgfbr2*$^{-/-}$ *Tbx21*$^{-/-}$ cells mainly via suppressing T_{Cir} gene expression.

These results demonstrate a hierarchy of interactions among TGF-β-induced T_{RM} differentiation events. TGF-β-induced T-bet downregulation and *Hic1* induction exert synergistic efforts leading to the formation of intestinal T_{RM}s.

DISCUSSION

TGF-β has been established as one of the key signals required for T_{RM} differentiation. The TGF-β-induced gene signature has been widely used in the T_{RM} field[26]; however, the key down-stream events mediated by TGF-β signaling required for T_{RM} differentiation are not entirely clear. Here, via a reductionist's approach, we sought to determine which TGF-β downstream events are critically involved in intestinal T_{RM} differentiation and can replace TGF-β signaling. We found that T-bet deficiency, but not Eomes deficiency, partially rescues intestinal T_{RM} differentiation in the absence of TGF-β signaling. This finding is

surprising as previous evidence supports a model that suppression of T-bet/Eomes sensitizes $CD8^+$ T cells to TGF-β signaling.[12] Our results demonstrate that T-bet deficiency can partially bypass TGF-β signaling. T-bet deficiency supports the formation of $CD103^+$ T_{RM}s in the absence of TGF-β receptor *in vivo*. However, T-bet deficiency cannot override the requirement of TGF-β signaling for CD103 induction *in vitro* or *ex vivo*. This finding suggests that a TGF-β-independent mechanism exists *in vivo* to support CD103 expression and intestinal T_{RM} differentiation, which is normally suppressed by T-bet. It will be interesting to define the molecular nature of this mechanism in the future.

Hic1 has been established as a key factor in promoting intestinal T_{RM} formation.[15] Here, we find that, during IEL T_{RM} differentiation, TGF-β induces and T-bet suppresses Hic1 expression. Based on a previous publication, Hic1 OE slightly reduces T-bet expression in $CD8^+$ T cells.[15] These findings suggest that T-bet downregulation and Hic1 induction are not entirely independent events. Importantly, Hic1 expression alone is sufficient to boost $CD69^+$ T_{RM} differentiation in the absence of TGF-β signaling. Interestingly, for the efficient formation of $CD69^+CD103^+$ mature T_{RM}s, both T-bet downregulation and Hic1 induction are required. Thus, it is highly possible that T-bet downregulation and Hic1 induction represent two essential events playing synergistic roles in TGF-β-mediated intestinal T_{RM} differentiation. Hic1 is also downstream of retinoic acid (RA) signaling. A recent publication has provided strong evidence that mesenteric lymph nodes provide essential RA signaling to license intestinal $CD103^+$ $CD8^+$ T_{RM} differentiation.[27] Whether enhanced RA signaling occurs in *Tgfbr2*$^{-/-}$ *Tbx21*$^{-/-}$ cells remains to be determined in the future.

How *Hic*1 OE enhances *Tgfbr2*$^{-/-}$ *Tbx21*$^{-/-}$ T_{RM} formation is not entirely clear. Our RNA-seq results suggest that *Hic1* OE inhibits the expression of circulation-related genes, consistent with its established role as a transcription repressor. However, this effect cannot fully explain the diverged overall gene expression pattern seen in the PCA plot (Figure 7A), which requires future investigation.

Even though T-bet deficiency supports the formation of $CD69^+CD103^+$ T_{RM}s in the absence of TGF-β receptor, the resulting *Tgfbr2*$^{-/-}$ *Tbx21*$^{-/-}$ T_{RM}s do carry important distinctions from WT T_{RM}s, such as enrichment of the type 17 effector program and high levels of Tcf-1 expression. It is interesting to note that both features are associated with T-bet deficiency and not unique to *Tgfbr2*$^{-/-}$ *Tbx21*$^{-/-}$ cells. Further, both features are not T_{RM}-specific as they are present in splenic memory T cells. We have shown that type 17 differentiation suppresses intestinal T_{RM} differentiation. Although the downregulation of Tcf-1 is required for the efficient formation of the T_{RM} population,[28] our results indicate that the high level of Tcf-1 expression in *Tgfbr2*$^{-/-}$ *Tbx21*$^{-/-}$ cells is not apparently involved in intestinal T_{RM} formation.

A recent publication using a commensal bacterial infection model has demonstrated that both T-bet-dependent type 1 T_{RM}s and c-Maf-dependent type 17 T_{RM}s are present in the skin.[29] Similar to *Tbx21*$^{-/-}$ $CD8^+$ T cells, *Tgfbr2*$^{-/-}$ *Tbx21*$^{-/-}$ $CD8^+$ T cells carry a clear type 17 signature. However, obvious distinctions exist between *Tgfbr2*$^{-/-}$ *Tbx21*$^{-/-}$ T_{RM}s in the gut and T_{RM}17 cells in the skin, including TGF-β dependency and the role of Tcf-1.

These distinctions may be due to the differences in infection models, tissues, or genetic models. Thus, the true molecular relationship between *Tgfbr2*$^{-/-}$ *Tbx21*$^{-/-}$ T_{RM}s in the small intestine and $T_{RM}1$/$T_{RM}17$ in the skin remains to be defined. It is conceivable that T_{RM}s isolated from different tissues require distinct transcriptional regulatory networks. For example, although the vast majority of T_{RM} subsets are TGF-β dependent, T_{RM}s isolated from the liver[26] and upper respiratory tract[30] are not. In addition, a CD69^{+}CD103^{-} T_{RM} subset in SI-LP is TGF-β independent and occupies a different microscopic location in an oral bacterial infection model[8]. It will be interesting to compare the location of *Tgfbr2*$^{-/-}$ *Tbx21*$^{-/-}$ T_{RM}s and WT controls in different infection models and further characterize their microenvironmental niches.

Together, using genetic models, we have identified T-bet downregulation and Hic1 induction as two distinct, yet critical, events downstream of TGF-β signaling during intestinal T_{RM} formation. Enforcing these two events allows intestinal T_{RM} differentiation in the absence of TGF-β signaling.

Limitation of the study

Our study is limited to one systemic viral infection model and P14 TCR transgenic cells. Different infection systems may yield different local environmental signals that affect T_{RM} differentiation. The findings presented in our study need to be validated in an oral-infection- or bacterial-infection-induced intestinal T_{RM} population. Our conditional-KO models are all mediated by distal *Lck*-Cre, which is active after thymocyte positive selection. This is not a T_{RM} stage-specific KO system. Indeed, we observed significant alterations in circulating memory T cells in the spleen. Further, we relied on a retrovirus-based delivery system to overexpress *Hic1* in CD8^{+} T cells. There are at least two caveats with this system. First, CD8^{+} T cells were activated *in vitro* before retrovirus transduction. Thus, the T cells were not primed *in vivo* in a physiological setting. Second, it is an OE system. The high level of enforced *Hic1* expression from an early-stage post-T cell priming may introduce unexpected confounding factors.

STAR★METHODS

RESOURCE AVAILABILITY

Lead contact—Further information and requests for resources and reagents should be directed to and will be fulfilled by the lead contact, Nu Zhang (zhangn3@uthscsa.edu).

Materials availability—This study did not generate new unique reagents.

Data and code availability

- The bulk RNA-seq data for splenic and SI-IEL P14 T cells are available for download on GEO data repository with accession number GSE184629. The bulk RNA-seq data for Hic OE P14 T cells available for download on GEO data repository with accession number GSE260630. The ATAC-seq results are available for download on GEO data repository with accession number GSE184628.

- This paper does not report original code.
- Any additional information required to reanalyze the data reported in this work paper is available from the lead contact upon request.

EXPERIMENTAL MODEL AND STUDY PARTICIPANT DETAILS

Mice and virus—C57BL/6J (B6) mice were obtained from the Jackson Laboratory and a colony of D^b-$GP_{33–41}$ TCR transgenic (P14) mice was maintained at our specific pathogen-free animal facilities at the University of Texas Health Science Center at San Antonio (San Antonio, Texas). B6.CD45.1 mice were originally obtained from the Jackson Laboratory and bred with P14 mice to generate congenically marked P14 mice. All recipient mice were used at 6 to 10 wk of age. *Tgfbr2*$^{f/f}$ and d*Lck*-Cre mice were described before[32,33] and available from Jax. *Tbx21*$^{f/f}$ (Jax#022741,[18]), *Eomes*$^{f/f}$ (Jax#017293,[34]) and *Rorc*$^{-/-}$ (Jax#007572,[35;36]) were purchased from Jackson Laboratory. Both male and female mice are used in the experiments. No sex-dependent difference was observed. All mice were housed at our specific pathogen-free animal facilities at the University of Texas Health at San Antonio (San Antonio, TX). All experiments were done in accordance with the University of Texas Health Science Center at San Antonio Institutional Animal Care and Use Committee guidelines. Mice were infected i.p. by 2×10^5 pfu LCMV Arm. Viruses were grown and quantified as described.[31]

Cell lines—293T cells (ATCC) were maintained in complete DMEM and used for retrovirus production.

METHOD DETAILS

Flow cytometry—Anti-CD16/32 (2.4G2) was produced in the lab and used in all FACS staining as FcR blocker. For intracellular cytokine staining, freshly isolated splenocytes were cultured with 0.1μM $GP_{33–41}$ peptide (AnaSpec) in the presence of Brefeldin A (BioLegend) for 4–5 h at 37°C. After surface staining, IFN—γ, TNF, IL-17 and IL-2 was performed using permeabilization buffer (BioLegend) following fixation. Ghost Dye Violet 510 (Tonbo Bioscience) was used to identify live cells. For granzyme staining, freshly isolated cells were surface stained, fixed and permeabilized using permeabilization buffer (BioLegend) before incubating with anti-granzyme antibodies. For transcription factor staining, surface-stained cells were treated by Foxp3/Transcription Factor Staining Buffer Kit (Tonbo). Washed and fixed samples were analyzed by BD LSRII or BD FACSCelesta, and analyzed by FlowJo (TreeStar) software.

Naive T cell isolation and adoptive transfer—Naive $CD8^+$ T cells were isolated from pooled spleen and lymph nodes using a MojoSort mouse CD8 T cell isolation kit (BioLegend) following the manufacturer's instruction. During the first step of biotin antibody cocktail incubation, biotin-αCD44 (IM7, BD) was added to label and deplete effector and memory T cells. Isolated naive $CD8^+$ T cells were enumerated, 1:1 mixed (WT P14 plus one of the KO/DKO P14 mice), 10^4 cells adoptively transferred into each sex-matched unmanipulated B6 recipient via an i.v. route before LCMV infection.

Lymphocyte isolation from the SI-IEL and SI-LP—Lymphocyte isolation procedures have been described before.[6,23] Briefly, small pieces of the small intestine were stirred at 800 rpm for 20 min in HBSS buffer containing 1mM dithiothreitol and 10% FCS at 37°C to release IEL. The remaining pieces of the small intestine were first treated by Ca^{2+}/Mg^{2+}-free HBSS containing 5mM EDTA to remove epithelia. EDTA-treated tissue was further digested by 0.08U/ml Liberase TL (Sigma, 5401020001) + 200U/ml DNase I (Sigma, D5025) + 1.33 mg/ml Dispase II (Sigma, D4693) with stirring for 45 min at 37°C. Both digested LP and released IEL were further purified by density gradient centrifugation with PBS-balanced 44% and 67% Percoll (Cytiva).

***In vitro* T cell activation—**Naive P14 T cells were stimulated with 10nM $GP_{33–41}$ peptide (AnaSpec) plus soluble 1 μg/ml αCD28 (37.51, Bio X Cell) in the presence of 5 ng/ml IL-2 (BioLegend) with 2.5 ng/ml added hTGF-β1 (Biolegend) or 10 μg/ml anti-TGF-β (1D11, BioXcell). 4 days after culture, the expression of CD103 was determined on live CD8 T cells by FACS.

***Ex vivo* effector T cell culture—**Day 5 post-LCMV Arm infection, total splenocytes containing P14 T cells were cultured in complete RPMI with 5 ng/ml IL-2 (BioLegend) in the presence or absence of added 20 ng/ml hTGF-β1 (Biolegend). 48 h later, the expression of CD103 on live P14 T cells was determined by FACS.

Retrovirus production and CD8 transduction—Retrovirus transduction was performed as described before.[37] Briefly, 293T cells were transfected with pCL-Eco and the plasmid of interest using FuGENE 6 (Promega). pCL-Eco was a gift from Inder Verma (Addgene).[38] MSCV-IRES-Thy1.1 DEST vector (Addgene)[39] was used to construct Hic1 OE vector. Retroviral supernatant was collected 48 h later. Purified naive P14 T cells were activated by 5 μg/ml αCD3+2 μg/ml αCD28 + 10 ng/ml IL-2 overnight. Live activated P14 T cells were purified by density gradient centrifugation with PBS-balanced 30% and 65% Percoll (Cytiva). Then, activated P14 T cells were spin infected by freshly collected retroviral supernatant in the presence of 4 μg/ml polybrene (Tocris) at 2,000g for 60 min at 30°C followed by 4-hour-incubation at 37°C. After extensive wash, $1×10^5$ retrovirus transduced P14 T cells were adoptively transferred into each recipient mouse, which had been infected by LCMV one day prior.

CRISPR/Cas9-mediated gene KO in naive T cells—We followed a published protocol using a Lonza 4D-Nucleofector and P3 primary cell 4D-Nucleofector X kit.[25] Pre-made Cas9 protein (IDT, Cat#1081059) and sgRNA (Synthego, CRISPRevolution sgRNA EZ kit) complex were prepared. Naive P14 T cells were resuspended in freshly prepared P3 buffer from P3 primary cell 4D-Nucleofector X kit. Resuspended cells were added to the preformed Cas9/sgRNA complex and were electroporated using a pre-configured program (Pulse DN100, for unstimulated mouse T cells). After electroporation, warm complete RPMI was added, and the cells were rested for 10 min in a cell culture incubator before live cell count and adoptive transfer.

RNA-seq analysis—Day 27 after infection, pooled P14 T cells from 5 to 10 recipient mice were isolated from SI-IEL compartment and FACS sorted into indicated subsets

based on congenic markers (CD45.1 and CD45.2) and T_{RM} markers (CD69 and CD103). Total RNA was extracted from sorted cells using a Quick-RNA Miniprep kit from Zymo Research. Sequencing library was constructed according to Illumina TruSeq Total RNA Sample Preparation Guide (RS-122–2201). Each library was barcoded and then pooled for cluster generation and sequencing run with 50bp single-end sequencing protocol on an Illumina HiSeq 3000 platform by UT Health San Antonio Genomic Sequencing Core Facility. An independent set of samples were sequenced by Novogene. Original RNA-seq results can be accessed by GSE184629. For Hic1 OE RNA-seq, retrovirus-transduced WT and *Tgfbr2*$^{-/-}$ *Tbx21*$^{-/-}$ P14 T cells were adoptively transferred into B6 recipients followed by LCMV infection. Twenty-two days later, SI-IEL lymphocytes were FACS sorted into 3 subsets, i.e., WT (with and without empty control retrovirus), *Tgfbr2*$^{-/-}$ *Tbx21*$^{-/-}$ (CD90.1^{-}, no retrovirus) and CD90.1^{+} *Tgfbr2*$^{-/-}$ *Tbx21*$^{-/-}$ (*Hic1* OE DKO). Total RNA was extracted from sorted cells and subjected to bulk RNA-seq analysis by Novogene. The results can be accessed by GSE260630.

For bioinformatic analysis, raw FASTQ files from RNA-Seq paired-end sequencing were trimmed and filtered by Fastp (version 0.19.5), and then aligned to the GRCm39/mm39 reference genome using Bowtie2 (version 2.4.1), the reads were counted by FeatureCounts (version 2.0.6). Genes with differential expression across samples (DEGs) were assessed using the DESeq2 (version 1.42.0) package of R. An FDR of 0.05 and Log2 fold change cut-off of 1 were imposed. PCA and heatmap plots were built using normalized and filtered log2 count. Gene set variation analysis (GSVA) and Rotation Gene Set Tests (Roast) were performed by the GSVA (version 1.50.0) and Limma (version 3.58.1) package in R, respectively. Gene Set Enrichment Analysis (GSEA) was performed using the Broad Institute software (https://www.broadinstitute.org/gsea/index.jsp). Multiple comparative analysis for T_{RM} and T_{Cir} were performed using published gene signatures.[4,40]

ATAC-seq analysis—ATAC-seq was performed as described before.[15] Briefly, 5×10^4 P14 T cells were FACS sorted from pooled samples. The nuclei pellet was treated with Tn5 transposase from Nextera DNA Sample Prep Kit (Illumina). The transposase-associated DNA was purified, amplified and then size selected before deep sequencing. Original ATAC-seq results can be accessed by GSE184628.

For bioinformatic analysis, raw ATAC-seq FASTQ files were trimmed and filtered by Fastp (version 0.19.5), and then aligned to the GRCm38/mm10 reference genome using Bowtie2 (version 2.4.1), the Samtools (version 1.3.1) were used to remove unmapped, unpaired, mitochondrial reads. PCR duplicates were removed using Picard (version 2.25.0). Peak calling was performed using Macs2 (version 2.2.7.1). For each experiment, we combined peaks of all samples to create a union peak list and merged overlapping peaks with BedTools (version 2.30.0) merge. The peaks were visualized in Integrative Genomics Viewer (IGV, version 2.9.4). The functional genomic regions of samples were visualized by ngsplot (https://github.com/shenlab-sinai/ngsplot). The motif analysis was performed using Homer (version 4.11).

QUANTIFICATION AND STATISTICAL ANALYSIS

Statistic details can be found in the figure legends. Mean ± SEM is shown in all figures. *p* value was calculated by two-tail paired or unpaired Student *t*-test or One-way ANOVA using Prism 10 software. *p* values of <0.05 were considered significant.

Supplementary Material

Refer to Web version on PubMed Central for supplementary material.

ACKNOWLEDGMENTS

This work is supported by NIH grants AI125701 and AI177345, a W. M. Keck Foundation award, and a VA merit award to N.Z. This work is also supported by NIH P01AI145815 to A.W.G. We thank Dr. Maximilian Heeg for suggestions about Hic1 staining. We thank Sebastian Montagnino for FACS sorting. Data were generated in the Flow Cytometry Shared Resource Facility, which is supported by the University of Texas Health Science Center at San Antonio, the Mays Cancer Center NIH/NCI grant P30 CA054174, and the National Center for Advancing Translational Sciences, National Institutes of Health, through grant UL1 TR002645. We thank Drs. Yidong Chen and Zhao Lai for bulk RNA-seq analysis. Data were generated in the Genome Sequencing Facility, which is supported by UT Health San Antonio, NIH-NCI P30 CA054174 (Cancer Center at UT Health San Antonio), NIH Shared Instrument grant 1S110OD021805-01 (S10 grant), and CPRIT Core Facility Award (RP160732).

DECLARATION OF INTERESTS

A.W.G. is a cofounder of TCura Bioscience, Inc. and serves on the scientific advisory boards of ArsenalBio and Foundery Innovations.

REFERENCES

1. Masopust D, and Soerens AG (2019). Tissue-Resident T Cells and Other Resident Leukocytes. Annu. Rev. Immunol. 37, 521–546. 10.1146/annurev-immunol-042617-053214. [PubMed: 30726153]
2. Mueller SN, and Mackay LK (2016). Tissue-resident memory T cells: local specialists in immune defence. Nat. Rev. Immunol. 16, 79–89. 10.1038/nri.2015.3. [PubMed: 26688350]
3. Milner JJ, and Goldrath AW (2018). Transcriptional programming of tissue-resident memory CD8(+) T cells. Curr. Opin. Immunol. 51, 162–169. 10.1016/j.coi.2018.03.017. [PubMed: 29621697]
4. Mackay LK, Rahimpour A, Ma JZ, Collins N, Stock AT, Hafon ML, Vega-Ramos J, Lauzurica P, Mueller SN, Stefanovic T, et al. (2013). The developmental pathway for CD103(+)CD8+ tissue-resident memory T cells of skin. Nat. Immunol. 14, 1294–1301. 10.1038/ni.2744. [PubMed: 24162776]
5. Sheridan BS, Pham QM, Lee YT, Cauley LS, Puddington L, and Lefrançois L. (2014). Oral infection drives a distinct population of intestinal resident memory CD8(+) T cells with enhanced protective function. Immunity 40, 747–757. 10.1016/j.immuni.2014.03.007. [PubMed: 24792910]
6. Zhang N, and Bevan MJ (2013). Transforming growth factor-beta signaling controls the formation and maintenance of gut-resident memory T cells by regulating migration and retention. Immunity 39, 687–696. 10.1016/j.immuni.2013.08.019. [PubMed: 24076049]
7. Hu Y, Lee YT, Kaech SM, Garvy B, and Cauley LS (2015). Smad4 promotes differentiation of effector and circulating memory CD8 T cells but is dispensable for tissue-resident memory CD8 T cells. J. Immunol 194, 2407–2414. 10.4049/jimmunol.1402369. [PubMed: 25637015]
8. Bergsbaken T, and Bevan MJ (2015). Proinflammatory microenvironments within the intestine regulate the differentiation of tissue-resident CD8(+) T cells responding to infection. Nat. Immunol 16, 406–414. 10.1038/ni.3108. [PubMed: 25706747]
9. El-Asady R, Yuan R, Liu K, Wang D, Gress RE, Lucas PJ, Dra-chenberg CB, and Hadley GA (2005). TGF-{beta}-dependent CD103 expression by CD8(+) T cells promotes selective destruction

of the host intestinal epithelium during graft-versus-host disease. J. Exp. Med 201, 1647–1657. 10.1084/jem.20041044. [PubMed: 15897278]

10. Intlekofer AM, Takemoto N, Wherry EJ, Longworth SA, Northrup JT, Palanivel VR, Mullen AC, Gasink CR, Kaech SM, Miller JD, et al. (2005). Effector and memory CD8+ T cell fate coupled by T-bet and eomesodermin. Nat. Immunol 6, 1236–1244. 10.1038/ni1268. [PubMed: 16273099]
11. Joshi NS, Cui W, Chandele A, Lee HK, Urso DR, Hagman J, Gapin L, and Kaech SM (2007). Inflammation directs memory precursor and short-lived effector CD8(+) T cell fates via the graded expression of T-bet transcription factor. Immunity 27, 281–295. 10.1016/j.immuni.2007.07.010. [PubMed: 17723218]
12. Mackay LK, Wynne-Jones E, Freestone D, Pellicci DG, Mielke LA, Newman DM, Braun A, Masson F, Kallies A, Belz GT, and Carbone FR (2015). T-box Transcription Factors Combine with the Cytokines TGF-beta and IL-15 to Control Tissue-Resident Memory T Cell Fate. Immunity 43, 1101–1111. 10.1016/j.immuni.2015.11.008. [PubMed: 26682984]
13. Fixemer J, Hummel JF, Arnold F, Klose CSN, Hofherr A, Weissert K, Kögl T, Kö ttgen M, Arnold SJ, Aichele P, and Tanriver Y. (2020). Eomes cannot replace its paralog T-bet during expansion and differentiation of CD8 effector T cells. PLoS Pathog. 16, e1008870. 10.1371/journal.ppat.1008870.
14. Schenkel JM, Fraser KA, Casey KA, Beura LK, Pauken KE, Vezys V, and Masopust D. (2016). IL-15-Independent Maintenance of Tissue-Resident and Boosted Effector Memory CD8 T Cells. J. Immunol 196, 3920–3926. 10.4049/jimmunol.1502337. [PubMed: 27001957]
15. Crowl JT, Heeg M, Ferry A, Milner JJ, Omilusik KD, Toma C, He Z, Chang JT, and Goldrath AW (2022). Tissue-resident memory CD8(+) T cells possess unique transcriptional, epigenetic and functional adaptations to different tissue environments. Nat. Immunol 23, 1121–1131. 10.1038/s41590-022-01229-8. [PubMed: 35761084]
16. Zhang N, and Bevan MJ (2012). TGF-beta signaling to T cells inhibits autoimmunity during lymphopenia-driven proliferation. Nat. Immunol 13, 667–673. 10.1038/ni.2319. [PubMed: 22634866]
17. Pritchard GH, Phan AT, Christian DA, Blain TJ, Fang Q, Johnson J, Roy NH, Shallberg L, Kedl RM, and Hunter CA (2023). Early T-bet promotes LFA1 upregulation required for CD8+ effector and memory T cell development. J. Exp. Med 220, e20191287. 10.1084/jem.20191287.
18. Intlekofer AM, Banerjee A, Takemoto N, Gordon SM, Dejong CS, Shin H, Hunter CA, Wherry EJ, Lindsten T, and Reiner SL (2008). Anomalous type 17 response to viral infection by CD8+ T cells lacking T-bet and eomesodermin. Science 321, 408–411. 10.1126/science.1159806. [PubMed: 18635804]
19. Milner JJ, Nguyen H, Omilusik K, Reina-Campos M, Tsai M, Toma C, Delpoux A, Boland BS, Hedrick SM, Chang JT, and Goldrath AW (2020). Delineation of a molecularly distinct terminally differentiated memory CD8 T cell population. Proc. Natl. Acad. Sci. USA 117, 25667– 25678. 10.1073/pnas.2008571117. [PubMed: 32978300]
20. Casey KA, Fraser KA, Schenkel JM, Moran A, Abt MC, Beura LK, Lucas PJ, Artis D, Wherry EJ, Hogquist K, et al. (2012). Antigen-independent differentiation and maintenance of effector-like resident memory T cells in tissues. J. Immunol 188, 4866–4875. 10.4049/jimmunol.1200402. [PubMed: 22504644]
21. Skon CN, Lee JY, Anderson KG, Masopust D, Hogquist KA, and Jameson SC (2013). Transcriptional downregulation of S1pr1 is required for the establishment of resident memory CD8+ T cells. Nat. Immunol 14, 1285–1293. 10.1038/ni.2745. [PubMed: 24162775]
22. Laidlaw BJ, Zhang N, Marshall HD, Staron MM, Guan T, Hu Y, Cauley LS, Craft J, and Kaech SM (2014). CD4+ T cell help guides formation of CD103+ lung-resident memory CD8+ T cells during influenza viral infection. Immunity 41, 633–645. 10.1016/j.immuni.2014.09.007. [PubMed: 25308332]
23. Liao W, Liu Y, Ma C, Wang L, Li G, Mishra S, Srinivasan S, Fan KKH, Wu H, Li Q, et al. (2021). The downregulation of IL-18R defines bona fide kidney-resident CD8(+) T cells. iScience 24, 101975. 10.1016/j.isci.2020.101975.
24. Thom JT, Weber TC, Walton SM, Torti N, and Oxenius A. (2015). The Salivary Gland Acts as a Sink for Tissue-Resident Memory CD8(+) T Cells, Facilitating Protection from Local

Cytomegalovirus Infection. Cell Rep. 13, 1125–1136. 10.1016/j.celrep.2015.09.082. [PubMed: 26526997]

25. Nussing S, House IG, Kearney CJ, Chen AXY, Vervoort SJ, Beavis PA, Oliaro J, Johnstone RW, Trapani JA, and Parish IA (2020). Efficient CRISPR/Cas9 Gene Editing in Uncultured Naive Mouse T Cells for In Vivo Studies. J. Immunol 204, 2308–2315. 10.4049/jimmunol.1901396. [PubMed: 32152070]
26. Christo SN, Evrard M, Park SL, Gandolfo LC, Burn TN, Fonseca R, Newman DM, Alexandre YO, Collins N, Zamudio NM, et al. (2021). Discrete tissue microenvironments instruct diversity in resident memory T cell function and plasticity. Nat. Immunol 22, 1140–1151. 10.1038/s41590-021-01004-1. [PubMed: 34426691]
27. Qiu Z, Khairallah C, Chu TH, Imperato JN, Lei X, Romanov G, Ata-kilit A, Puddington L, and Sheridan BS (2023). Retinoic acid signaling during priming licenses intestinal CD103+ CD8 TRM cell differentiation. J. Exp. Med 220, e20210923. 10.1084/jem.20210923.
28. Wu J, Madi A, Mieg A, Hotz-Wagenblatt A, Weisshaar N, Ma S, Mohr K, Schlimbach T, Hering M, Borgers H, and Cui G. (2020). T Cell Factor 1 Suppresses CD103+ Lung Tissue-Resident Memory T Cell Development. Cell Rep. 31, 107484. 10.1016/j.celrep.2020.03.048.
29. Park SL, Christo SN, Wells AC, Gandolfo LC, Zaid A, Alexandre YO, Burn TN, Schröder J, Collins N, Han SJ, et al. (2023). Divergent molecular networks program functionally distinct CD8(+) skin-resident memory T cells. Science 382, 1073–1079. 10.1126/science.adi8885. [PubMed: 38033053]
30. Pizzolla A, Nguyen THO, Smith JM, Brooks AG, Kedzieska K, Heath WR, Reading PC, and Wakim LM (2017). Resident memory CD8(+) T cells in the upper respiratory tract prevent pulmonary influenza virus infection. Sci. Immunol 2, eaam6970. 10.1126/sciimmunol.aam6970.
31. Ma C, Mishra S, Demel EL, Liu Y, and Zhang N. (2017). TGF-beta Controls the Formation of Kidney-Resident T Cells via Promoting Effector T Cell Extravasation. J. Immunol 198, 749–756. 10.4049/jimmunol.1601500. [PubMed: 27903738]
32. Leveen P, Carlsen M, Makowska A, Oddsson S, Larsson J, Goumans M-J, Cilio CM, and Karlsson S. (2005). TGF-beta type II receptor-deficient thymocytes develop normally but demonstrate increased CD8+ proliferation in vivo. Blood 106, 4234–4240. 10.1182/blood-2005-05-1871. [PubMed: 16131565]
33. Zhang DJ, Wang Q, Wei J, Baimukanova G, Buchholz F, Stewart AF, Mao X, and Killeen N. (2005). Selective expression of the Cre recombinase in late-stage thymocytes using the distal promoter of the Lck gene. J. Immunol 174, 6725–6731. 10.4049/jimmunol.174.11.6725. [PubMed: 15905512]
34. Zhu Y, Ju S, Chen E, Dai S, Li C, Morel P, Liu L, Zhang X, and Lu B. (2010). T-bet and eomesodermin are required for T cell-mediated anti-tumor immune responses. J. Immunol 185, 3174–3183. 10.4049/jimmunol.1000749. [PubMed: 20713880]
35. Eberl G, Marmon S, Sunshine MJ, Rennert PD, Choi Y, and Littman DR (2004). An essential function for the nuclear receptor RORgamma(t) in the generation of fetal lymphoid tissue inducer cells. Nat. Immunol 5, 64–73. 10.1038/ni1022. [PubMed: 14691482]
36. Ivanov II, McKenzie BS, Zhou L, Tadokoro CE, Lepelley A, Lafaille JJ, Cua DJ, and Littman DR (2006). The orphan nuclear receptor RORgammat directs the differentiation program of proinflammatory IL-17+ T helper cells. Cell 126, 1121–1133. 10.1016/j.cell.2006.07.035. [PubMed: 16990136]
37. Kurachi M, Kurachi J, Chen Z, Johnson J, Khan O, Bengsch B, Stelekati E, Attanasio J, McLane LM, Tomura M, et al. (2017). Optimized retroviral transduction of mouse T cells for in vivo assessment of gene function. Nat. Protoc 12, 1980–1998. 10.1038/nprot.2017.083. [PubMed: 28858287]
38. Naviaux RK, Costanzi E, Haas M, and Verma IM (1996). The pCL vector system: rapid production of helper-free, high-titer, recombinant retroviruses. J. Virol 70, 5701–5705. 10.1128/JVI.70.8.5701-5705.1996. [PubMed: 8764092]
39. Wu Y, Borde M, Heissmeyer V, Feuerer M, Lapan AD, Stroud JC, Bates DL, Guo L, Han A, Ziegler SF, et al. (2006). FOXP3 controls regulatory T cell function through cooperation with NFAT. Cell 126, 375–387. 10.1016/j.cell.2006.05.042. [PubMed: 16873067]

40. Mackay LK, Minnich M, Kragten NAM, Liao Y, Nota B, Seillet C, Zaid A, Man K, Preston S, Freestone D, et al. (2016). Hobit and Blimp1 instruct a universal transcriptional program of tissue residency in lymphocytes. Science 352, 459–463. 10.1126/science.aad2035. [PubMed: 27102484]

Highlights

- T-bet deficiency partially rescues TGF-βR-KO T_{RM} formation in the small intestine
- T-bet-deficiency-induced type 17 program inhibits gut T_{RM} formation
- Hic1 further boosts gut T_{RM} differentiation in the absence of TGF-β receptor

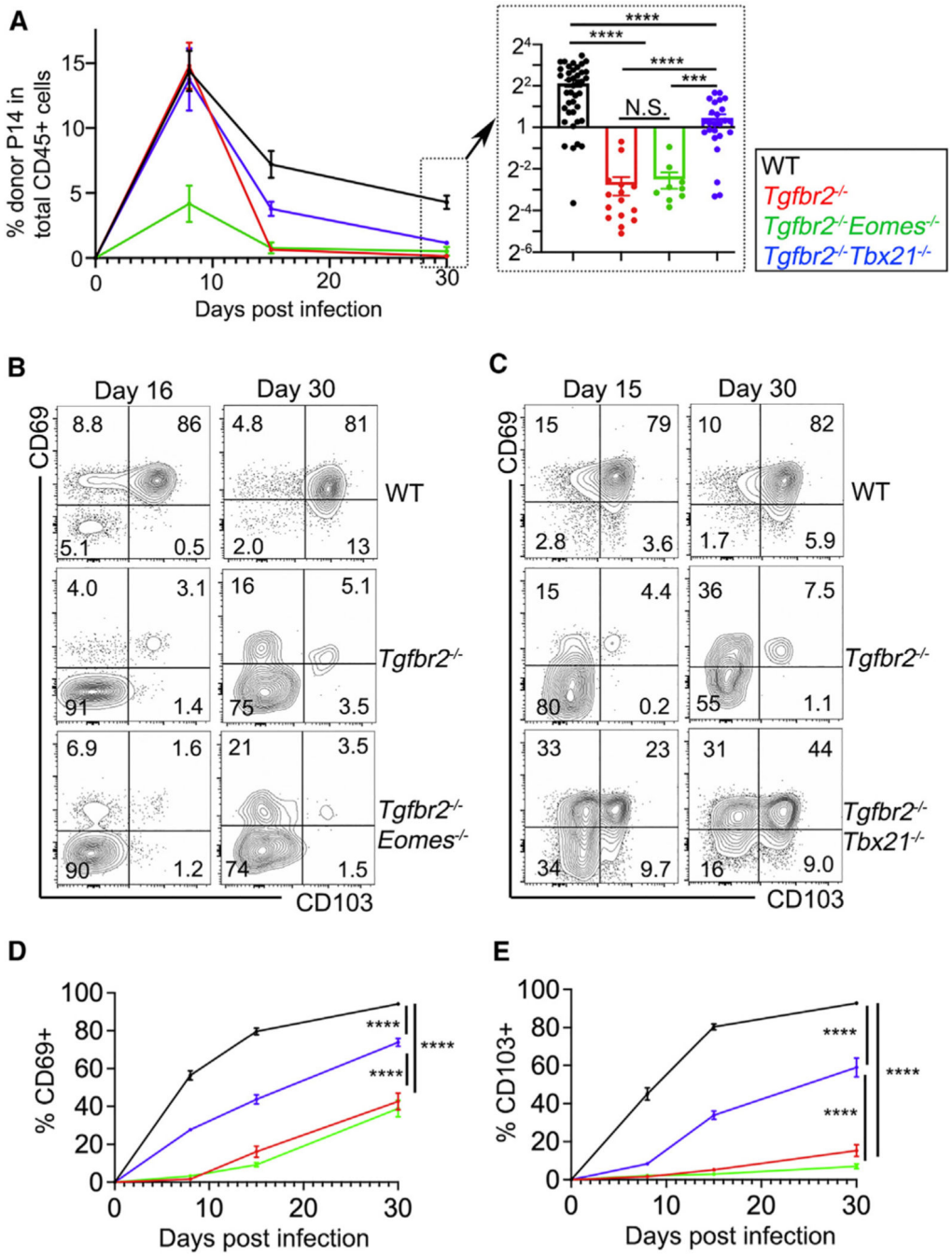

Figure 1. T-bet deficiency, but not Eomes deficiency, rescues gut-resident memory T cell differentiation in the absence of TGF-β receptor

Same experimental setup as in Figure S2A.

(A) The percentage of donor P14 T cells in the total CD45$^+$ cell population isolated from SI-IEL is shown (n = 8–37 individual recipient mice for each time point). Day 30 results are presented as a bar graph. (B and C) Representative FACS profiles of pre-gated donor P14 T cells isolated from SI-IEL are shown. (D and E) (D) The percentage of CD69$^+$ and (E) CD103$^+$ cells in donor P14 T cells isolated from SI-IEL are shown (n = 5–30). Mean ± SEM is shown for each data point in (A), (D), and (E). Pooled results from three to six

independent experiments are shown in (A), (D), and (E). N.S., not significant; ***$p < 0.001$; and ****$p < 0.0001$ by ordinary one-way ANOVA with multiple-comparison post test for the last time point.

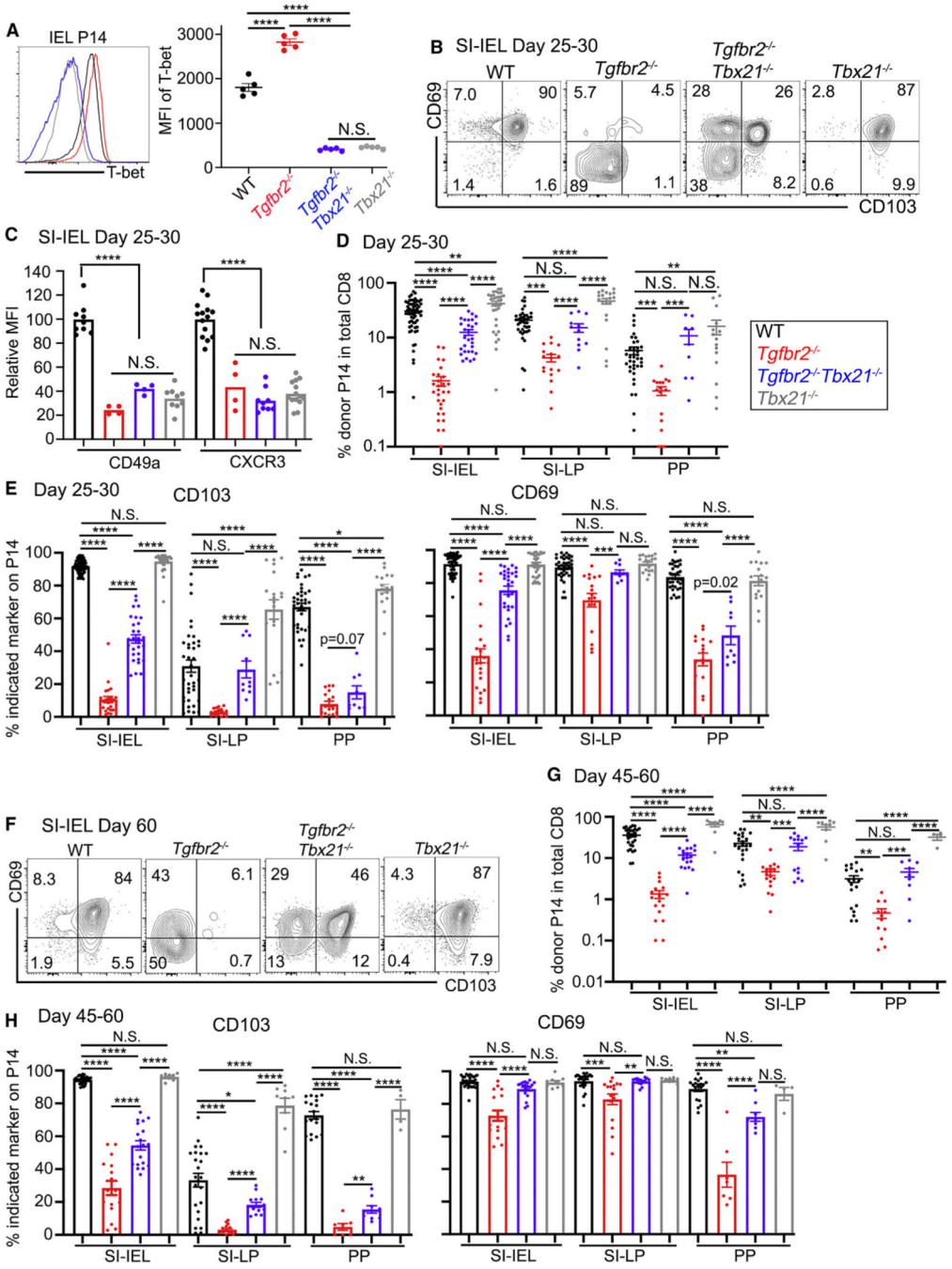

Figure 2. T-bet deficiency partially overcomes the differentiation block in *Tgfbr2*$^{-/-}$ cells

Similar experimental setup as in Figure S2A.

(A) Day 7 post infection, the expression of T-bet in SI-IEL P14 T cells was measured by flow cytometry ($n = 5$).

(B–H) (B–E) Day 25–30 post infection, (F) to (H) day 45–60 post infection. (B and F) Representative FACS profiles of pre-gated donor P14 T cells isolated from SI-IEL are shown. (C) MFI of CD49a and CXCR3 on pre-gated SI-IEL P14 T cells are shown (n = 4–14). (D and G) The percentage of donor P14 T cells in total CD8 is shown. (E and H) The

percentages of $CD103^+$ (left) and $CD69^+$ (right) in donor P14 T cells are shown ($n = 9–57$ for D and E; $n = 4–29$ for G and H). Each symbol represents the results of an individual mouse. Mean ± SEM is shown. Pooled results from two to six independent experiments are shown. N.S., not significant; *$p < 0.05$; **$p < 0.01$; ***$p < 0.001$; and ****$p < 0.0001$ by ordinary one-way ANOVA with multiple-comparison post test or Student t test.

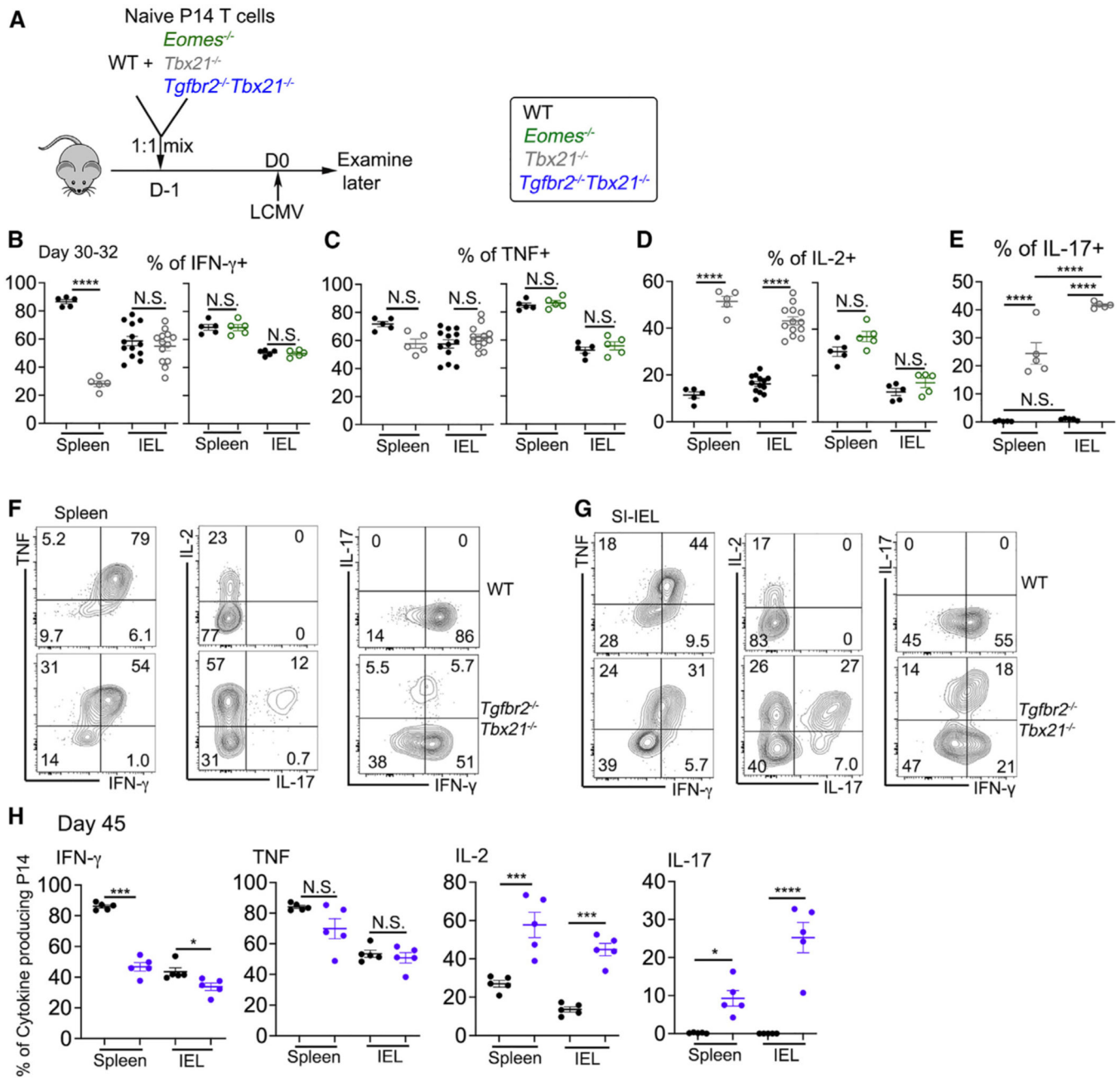

Figure 3. *Tgfbr2*$^{-/-}$*Tbx21*$^{-/-}$ gut-resident memory T cells exhibit an altered effector program

(A) Schematics. Naive P14 isolated from WT and one of the KOs (gray *Tbx21*$^{-/-}$, green *Eomes*$^{-/-}$, and blue *Tgfbr2*$^{-/-}$*Tbx21*$^{-/-}$) were co-transferred into B6 recipients followed by LCMV infection.

(B–H) Day 30–32 (B–E) or day 45 post infection (F–H), the percentage of cytokine-producing P14 T cells are shown in (B)–(E) and (H). Representative FACS profiles of pre-gated donor P14 T cells isolated from the spleen (F) and SI-IEL (G) are shown. Each symbol in(B)–(E) and (H) represents the results from an individual recipient mouse (n = 5–13). Mean ± SEM is shown. N.S., not significant; *$p < 0.05$; ***$p < 0.001$; and ****$p < 0.0001$ by ordinary one-way ANOVA with multiple-comparison post test.

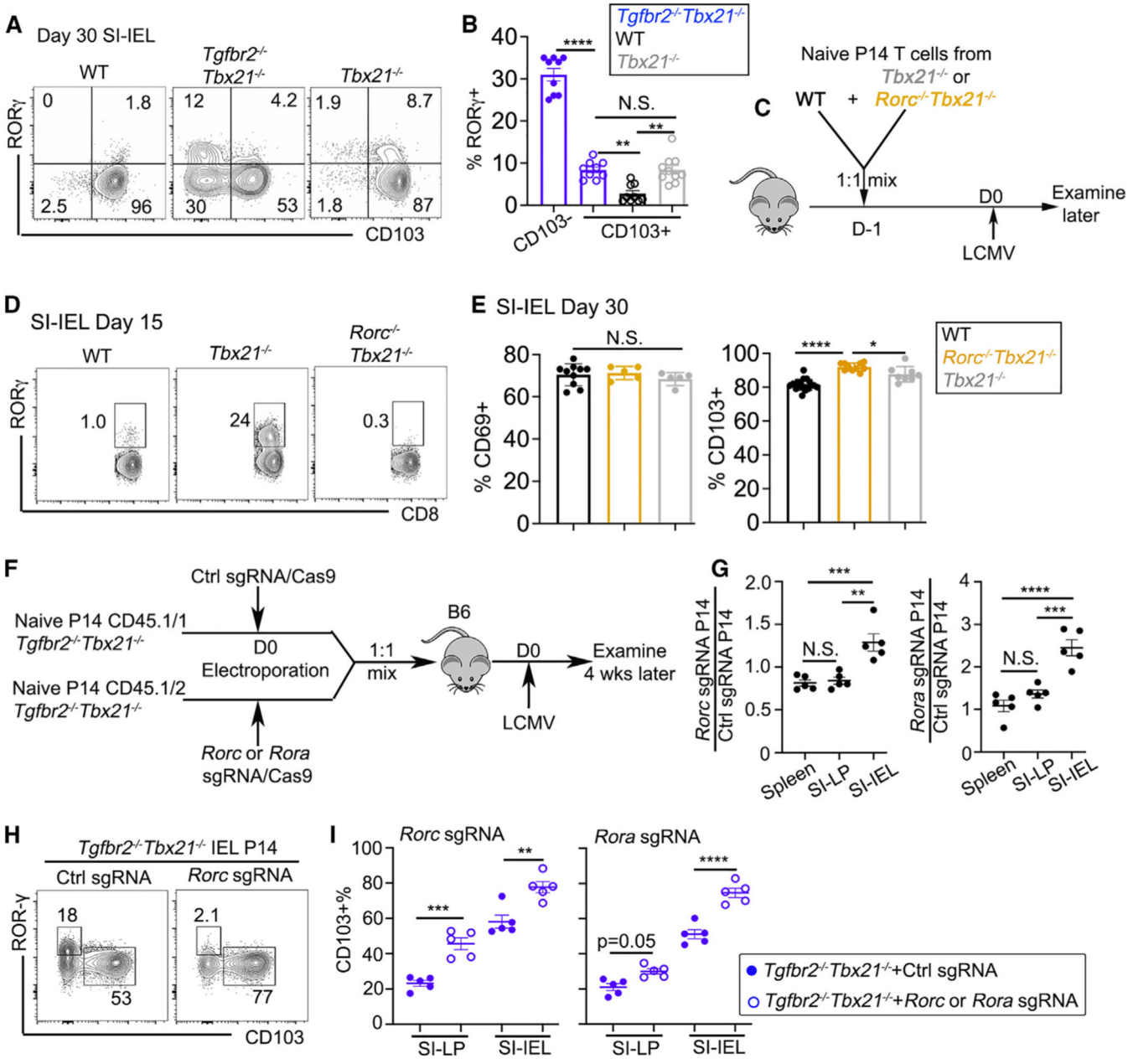

Figure 4. Type 17 program suppresses gut T_{RM} in the absence of T-bet

Similar experimental setup as in Figure S2A.

(A) Representative FACS profiles of pre-gated donor P14 T cells isolated from SI-IEL are shown.

(B) The percentage of RORγ$^+$ cells in each subset of SI-IEL P14 T cells at day 30 post infection (n = 9–10).

(C) Schematics for the experiments shown in (D) and (E).

(D) Representative FACS profiles of pre-gated SI-IEL P14 T cells are shown.

(E) The percentage of CD69$^+$ (left, n = 5–10) and CD103$^+$ (right, n = 8–18) cells in donor P14 T cells isolated from SI-IEL at day 30 post infection are shown.

(F) Schematics for the experiments shown in (G)–(I).

(G) The ratio of Cas9-mediated KO P14s over co-transferred control P14s is shown. Left, *Rorc*-sgRNA; right, *Rora*-sgRNA ($n = 5$).

(H) Representative FACS plots to show the deletion efficiency of *Rorc* in IEL P14 T cells.

(I) The percentage of $CD103^+$ cells in gut P14 T cells are shown ($n = 5$). Each symbol in (B), (E), (G), and (I) represents the results from an individual mouse. Mean ± SEM is shown. Pooled results from two independent experiments are shown. N.S., not significant; $*p < 0.05$; $**p < 0.01$; $***p < 0.001$; and $****p < 0.0001$ by ordinary one-way ANOVA with multiple-comparison post test.

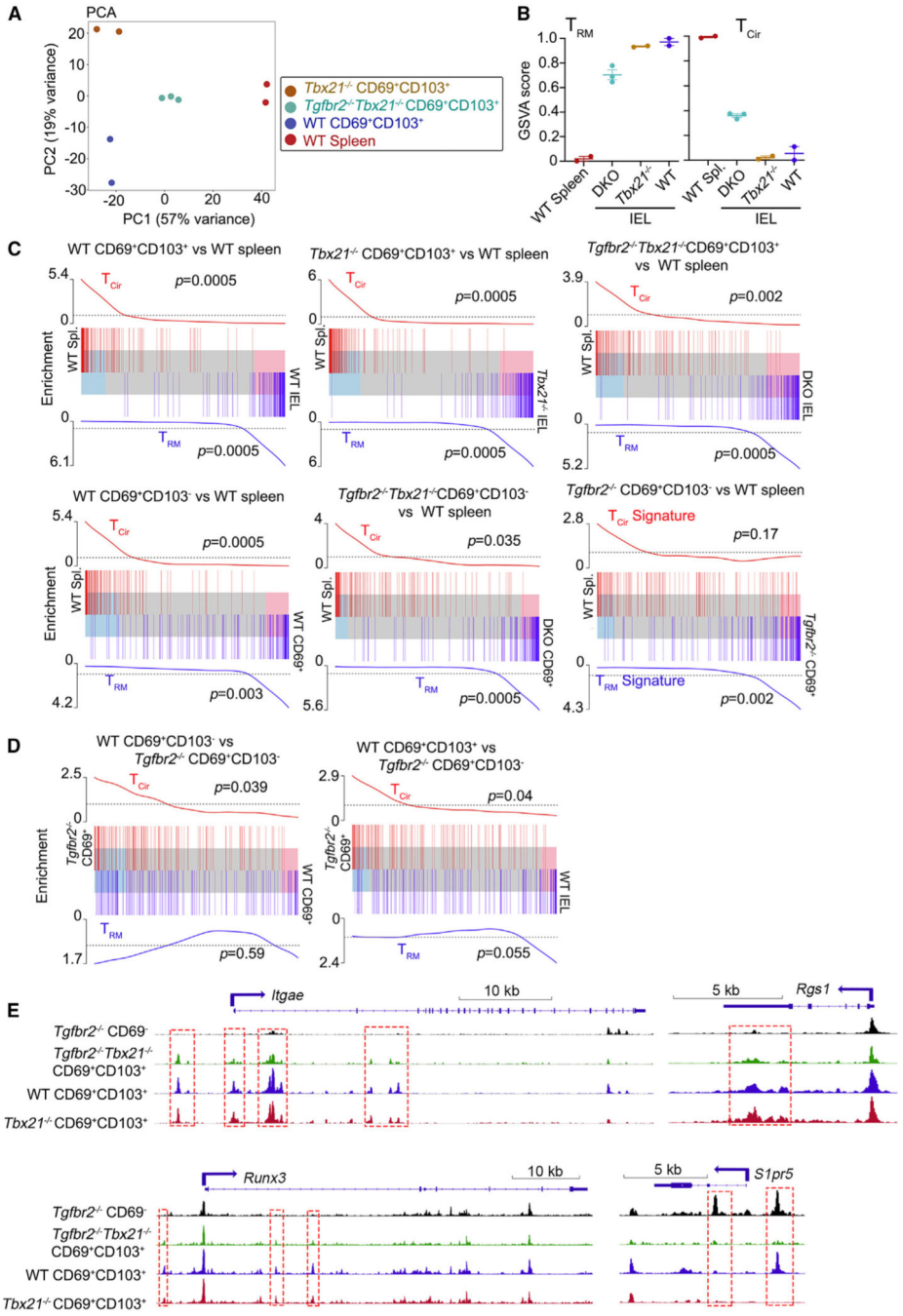

Figure 5. T-bet deficiency partially overcomes the transcriptional and epigenetic blocks in IEL T_{RM} differentiation in the absence of TGF-β signaling

Various subsets of FACS-sorted P14 T cells were subjected to bulk RNA-seq and ATAC-seq analysis.

(A) Principal-component analysis (PCA) of RNA-seq results is shown.

(B) GSVA scores for T_{RM} signature (left) and T_{Cir} signature (right) are calculated based on RNA-seq results. Each symbol represents a biologically independent replicate.

(C and D) GSEA for circulating T cell signature genes and SI-IEL T_{RM} signature genes.

(E) ATAC-seq results for representative T_{RM}-related loci are shown.

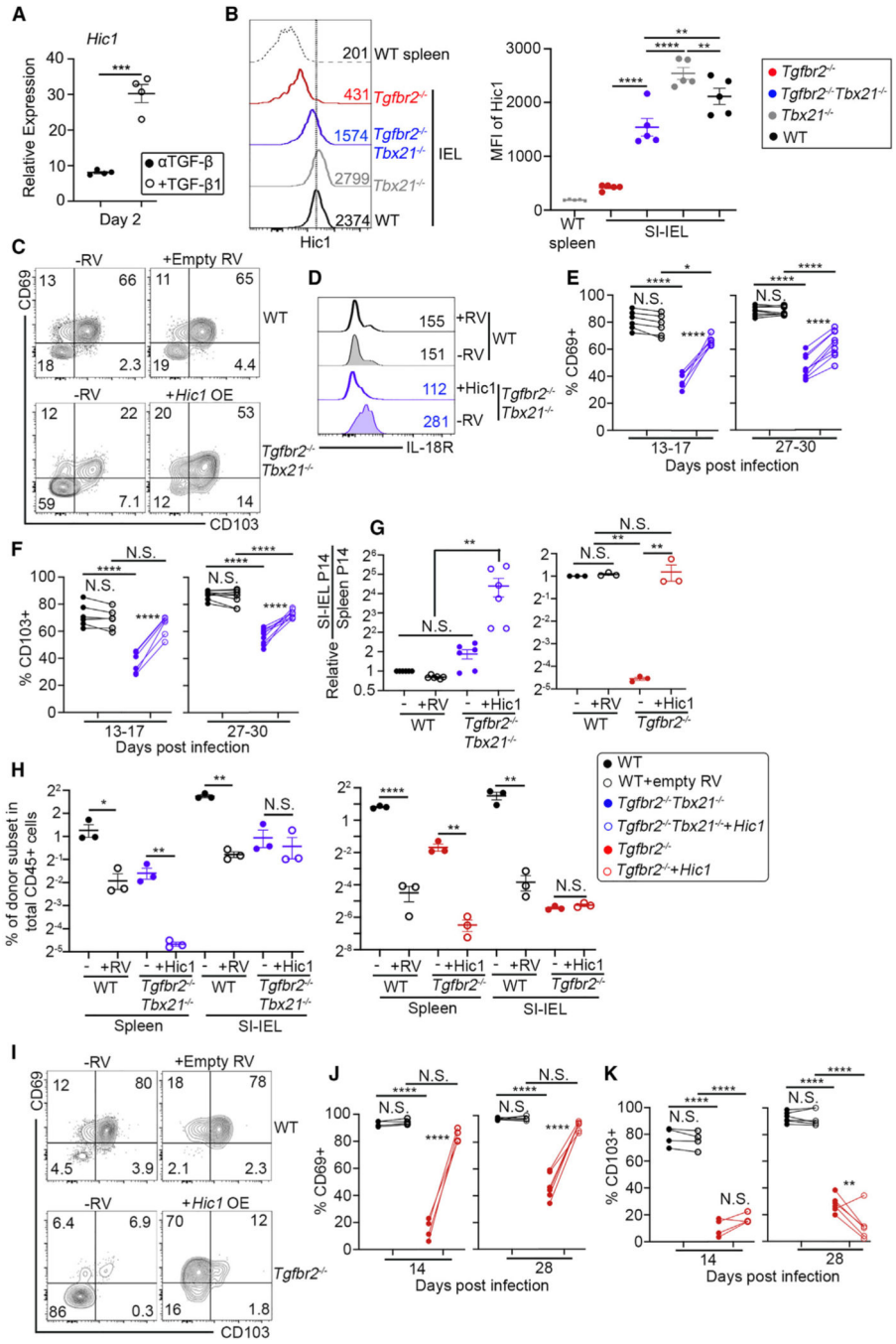

Figure 6. *Hic1* OE and T-bet downregulation cooperate to mediate TGF-β-induced T_{RM} differentiation program

(A) Purified WT naive $CD8^+$ T cells were activated *in vitro* with TGF-β-neutralizing antibody or added TGF-β. *Hic1* expression was measured by bulk RNA-seq ($n = 4$ independent replicates).

(B) Similar setup as in Figure S2A. Day 20 post infection, Hic1 expression in donor P14 T cells was measured by FACS ($n = 5$).

(C–K) (C and D) d13 and (I) d14 post infection, representative FACS of pre-gated IEL P14 subsets are shown. Numbers in (B) and (D) represent MFI. (E and J) The percentage

of $CD69^+$ and (F and K) the percentage of $CD103^+$ cells in each IEL P14 subset are shown (n = 6–9 for E and F; n = 4–6 for J and K). D27–30 post infection, the relative population size of each IEL P14 subset (G) and the percentage of each donor subset in total $CD45^+$ cells (H) are shown (n = 3–6). Each symbol and each pair of symbols represent the results from an individual recipient mouse. Mean ± SEM is shown. Pool results from two or three independent experiments are shown for each setting. N.S., not significant; *p < 0.05; **p < 0.01; ***p < 0.001; and ****p < 0.0001 by ordinary one-way ANOVA with multiple-comparison post test or Student t test.

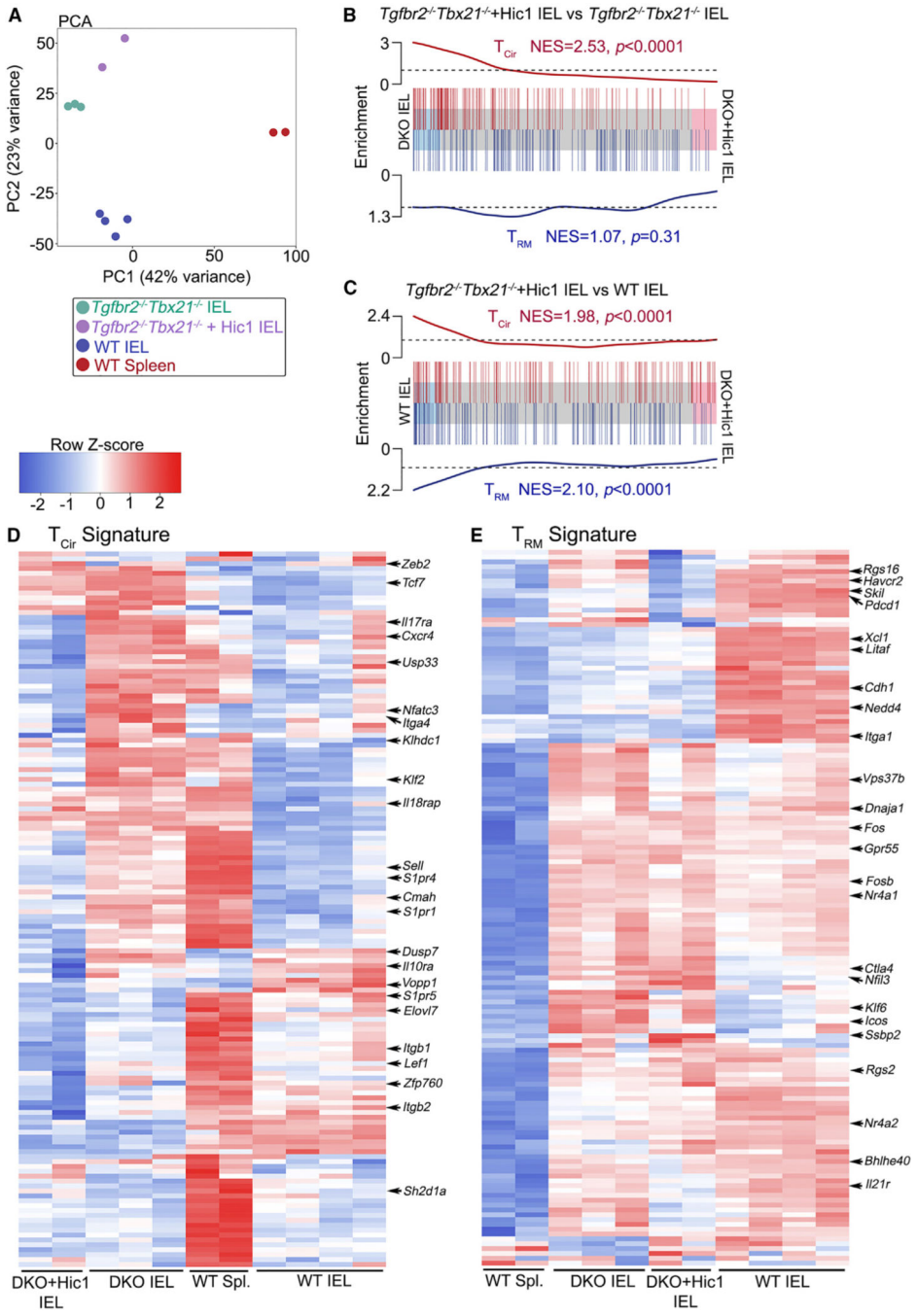

Figure 7. *Hic1* overexpression suppresses the expression of circulating genes in *Tgfbr2*$^{-/-}$*Tbx21*$^{-/-}$ T cells

WT and *Tgfbr2*$^{-/-}$ *Tbx21*$^{-/-}$ P14 T cells were transduced by retrovirus before being co-transferred into LCMV-infected recipients. D22 post transfer, different subsets of IEL P14 T cells were FACS sorted and subjected to bulk RNA-seq.

(A) PCA plot is shown. GSEA for T_{Cir} and T_{RM} signatures between *Tgfbr2*$^{-/-}$ *Tbx21*$^{-/-}$ and *Tgfbr2*$^{-/-}$ *Tbx21*$^{-/-}$ Hic1 OE (B) and *Tgfbr2*$^{-/-}$ *Tbx21*$^{-/-}$ Hic1 OE and WT (C). Heatmap

focused on T_{Cir} signature genes (D) and T_{RM} signature genes (E). Each column represents a biologically independent replicate.

KEY RESOURCES TABLE

REAGENT or RESOURCE	SOURCE	IDENTIFIER
Antibodies		
PE anti-CD127 (A7R34)	BioLegend	Cat#135009; RRID: AB_1937252
PerCP/Cyanine 5.5 anti-CD127 (A7R34)	BioLegend	Cat#135022; RRID: AB_1937273
APC anti-CD127 (A7R34)	BioLegend	Cat#135012; RRID: AB_1937216
Brilliant Violet 785™ anti-CD127 (A7R34)	BioLegend	Cat# 135037; RRID: AB_2565269
Ultra-LEAF™ Purified anti-CD3e (145–2C11)	BioLegend	Cat# 100359; RRID: AB_2616673
InVivoMAb anti-CD28 (37.51)	Bio X Cell	Cat#BE0015–1; RRID: AB_1107624
APC anti-KLRG1 (2F1)	Cytek (Tonbo)	Cat#20–5893-U100; RRID: AB_2621607
PE/Cyanine7 anti-KLRG1 (2F1)	BioLegend	Cat#138416; RRID: AB_2561736
Brilliant Violet 605™ anti-KLRG1 (2F1)	BioLegend	Cat#138419; RRID: AB_2563357
FITC anti-CD8b (H35–17.2)	Thermo Fisher Scientific	Cat#11–0083-85; RRID: AB_657764
APC-eFluor™ 780 anti-CD8b (H35–17.2)	Thermo Fisher Scientific	Cat#47–0083-82; RRID: AB_2573943
eFluor™ 450 anti-CD8b (H35–17.2)	Thermo Fisher Scientific	Cat#48–0083-82; RRID: AB_11218504
PE anti-CD8b (YTS156.7.7)	BioLegend	Cat#126608; RRID: AB_961298
PerCP/Cyanine5.5 anti-CD45.1 (A20)	Cytek (Tonbo)	Cat#65–0453-U100; RRID: AB_2621893
APC/Cyanine7 anti-CD45.1 (A20)	Cytek (Tonbo)	Cat#25–0453-U100; RRID: AB_2621629
APC anti-CD45.1 (A20)	BioLegend	Cat#110714; RRID: AB_313503
Super Bright™ 600 anti-CD45.1 (A20)	Thermo Fisher Scientific	Cat#63–0453-82; RRID: AB_2717041
APC anti-CD45.2 (104)	BioLegend	Cat#109814; RRID: AB_389211
FITC anti-CD45.2 (104)	BioLegend	Cat#109806; RRID: AB_313443
PE/Cyanine7 anti-CD45.2 (104)	Cytek (Tonbo)	Cat#60–0454-U100; RRID: AB_2621851
APC/Cyanine7 anti-CD45.2 (104)	Cytek (Tonbo)	Cat#25–0454-U100; RRID: AB_2621630
Super Bright™ 780 anti-CD45.2 (104)	Thermo Fisher Scientific	Cat#78–0454-82; RRID: AB_2802469
FITC anti-CD62L (MEL-14)	Cytek (Tonbo)	Cat#35–0621-U500; RRID: AB_2621697
APC/Fire™ 750 anti-CD62L (MEL-14)	BioLegend	Cat#104450; RRID: AB_2629772
PE anti-CD69 (H1.2F3)	BioLegend	Cat#104508; RRID: AB_313111
APC anti-CD69 (H1.2F3)	BioLegend	Cat#104514; RRID: AB_492843
PE/Cyanine7 anti-CD69 (H1.2F3)	Cytek (Tonbo)	Cat#60–0691-U100; RRID: AB_2621856

REAGENT or RESOURCE	SOURCE	IDENTIFIER
Super Bright™ 600 anti-CD69 (H1.2F3)	Thermo Fisher Scientific	Cat#63–0691-82; RRID: AB_2688097
APC anti-CD183 (CXCR3–173)	BioLegend	Cat#126512; RRID: AB_1088993
Alexa Fluor® 647 anti-CD103 (2E7)	BioLegend	Cat#121410; RRID: AB_535952
PerCP/Cyanine5.5 anti-CD103 (2E7)	BioLegend	Cat#121416; RRID: AB_2128621
PE anti-CD103 (2E7)	Thermo Fisher Scientific	Cat#12–1031-83; RRID: AB_465799
Super Bright™ 600 anti-CD103 (2E7)	Thermo Fisher Scientific	Cat#63–1031-82; RRID: AB_2802433
PE anti-CD218a (P3TUNYA)	Thermo Fisher Scientific	Cat#12–5183-82; RRID: AB_2572617
eFluor™ 450 anti-CD218a (P3TUNYA)	Thermo Fisher Scientific	Cat#48–5183-82; RRID: AB_2574069
APC/Cyanine7 anti-CD90.1 (OX-7)	BioLegend	Cat#202519; RRID: AB_2201418
PE anti-CD49a (HMa1)	BioLegend	Cat#142603; RRID: AB_10945160
PE/Cyanine7 anti-IFN-g (XMG1.2)	BioLegend	Cat#505826; RRID: AB_2295770
Brilliant Violet 605™ anti-IFN-g (XMG1.2)	BioLegend	Cat#505840; RRID: AB_2734493
PE anti-IL-2 (JES6–5H4)	BioLegend	Cat#503808; RRID: AB_315302
Pacific Blue™ anti-TNF-a (MP6-XT22)	BioLegend	Cat#506318; RRID: AB_893639
FITC anti-TNF-a (MP6-XT22)	BioLegend	Cat#506304; RRID: AB_315425
Alexa Fluor® 488 anti-IL-17A (TC11–18H10.1)	BioLegend	Cat#506909; RRID: AB_536011
PE/Cyanine7 anti-Granzyme A (GzA-3G8.5)	Thermo Fisher Scientific	Cat#25–5831-82; RRID: AB_2573476
PE anti-Granzyme A (GzA-3G8.5)	Thermo Fisher Scientific	Cat#12–5831-82; RRID: AB_2572631
PE anti-RORgt (AFKJS-9)	Thermo Fisher Scientific	Cat#12–6988-82; RRID: AB_1834470
Anti-CD16/32 (2.4G2)	Produced in-house	N/A
FITC anti-T-bet (4B10)	BioLegend	Cat#644811; RRID: AB_2287097
PE anti-T-bet (4B10)	Thermo Fisher Scientific	Cat#12–5825-82; RRID: AB_925761
PE anti-Eomes (Dan11mag)	Thermo Fisher Scientific	Cat#12–4875-82; RRID: AB_1603275
Alexa Fluor™ 488 anti-Eomes (Dan11mag)	Thermo Fisher Scientific	Cat#53–4875-82; RRID: AB_10854265
Alexa Fluor® 488 anti-TCF1/TCF7 (C63D9)	Cell Signaling Tech	Cat#6444S; RRID: AB_2797627
Pacific Blue™ anti-TCF1/TCF7 (C63D9)	Cell Signaling Tech	Cat#9066S; RRID: AB_2797696
Alexa Fluor®647 anti-TCF1/TCF7 (C63D9)	Cell Signaling Tech	Cat#6709S; RRID: AB_2797631
Biotin anti-CD44 (IM7)	BD Biosciences	Cat#553132; RRID: AB_394647
InVivoMAb Anti-TGF-β (1D11.16.8)	Bio X Cell	Cat#BE0057; RRID: AB_1107757
Alexa Fluor®647 anti-Hic1 (H-6)	Santa Cruz	Cat#sc-271499; RRID: AB_10650134

REAGENT or RESOURCE	SOURCE	IDENTIFIER
MSCV-IRES-Thy1.1 DEST	Addgene	Addgene plasmid #17442; RRID: Addgene_17442
MSCV-Hic1-IRES-Thy1.1	This paper	N/A
Software and algorithms		
FlowJo v10	Treestar Inc	RRID:SCR_008520
Prism 10	Graphpad Inc	RRID:SCR_002798
Fastp (version 0.19.5)	Anaconda	RRID:SCR_016962
Bowtie 2 (version 2.4.1)	Anaconda	RRID:SCR_016368
Subread (version 2.0.6)	Anaconda	RRID:SCR_009803
Macs2 (version 2.2.7.1)	Anaconda	RRID:SCR_013291
Samtools (version 1.3.1)	Anaconda	RRID:SCR_002105
Picard (version 2.25.0)	Anaconda	RRID:SCR_006525
BedTools (version 2.30.0)	Anaconda	RRID:SCR_006646
Homer (version 4.11)	Anaconda	RRID:SCR_010881
R (version 4.3.1)	R Foundation	RRID:SCR_001905
DESeq2 (version 1.42.0)	Bioconductor	RRID:SCR_015687
GSVA (version 1.50.0)	Bioconductor	RRID:SCR_021058
Limma (version 3.58.1)	Bioconductor	RRID:SCR_010943
Gene Set Enrichment Analysis (version 4.2.2)	Broad Institute	RRID:SCR_003199
ngsplot	shenlab	RRID:SCR_011795
Integrative Genomics Viewer (version 2.9.4)	Broad Institute	RRID:SCR_011793